

1 21 Oct 09

Submitted to JGR-Atmospheres

2 **Gravity and Rossby Wave Signatures in the Tropical Troposphere and Lower**
3 **Stratosphere Based on Southern Hemisphere Additional Ozonesondes (SHADOZ),**
4 **1998-2007**

5 Anne M. Thompson^{1*}, Amber L. Allen², Sukyoung Lee¹, Sonya K. Miller¹, Jacquelyn C.
6 Witte³

7 ¹ Dept of Meteorology, The Pennsylvania State University, 503 Walker Bldg, University
8 Park, PA 16802-5013; amt16@psu.edu, sl@meteo.psu.edu, smiller@meteo.psu.edu;
9 814-865-0479

10 ² Dept of Meteorology, The Pennsylvania State University; now at ERG, 1600 Perimeter
11 Park Drive, Morrisville, NC 27560; 919-468-7889; amber.allen@erg.com

12 ³ SSAI, Lanham, MD 20706; also at NASA/Goddard/Code 613.3, Greenbelt, MD 20771;
13 301-614-5731; jacquelyn.witte@nasa.gov

14 *Corresponding Author

15 Index Terms: 0368, 3314, 3334, 3362, 3374

16 Keywords: tropical tropopause layer, ozonesondes, tropical convection, ENSO, gravity
17 waves

18 **ABSTRACT**

19 Prior investigations have attempted to determine the relative influence of advection and
20 convective processes on ozone and water vapor distributions in the tropical tropical
21 tropopause layer (TTL) through analyses of tracers, related physical parameters (e.g., out-
22 going long-wave radiation, precipitable water, temperature) and with models. In this study,
23 stable laminae in Southern Hemisphere Additional Ozonesonde Network (SHADOZ) ozone
24 profiles from 1998-2007 are interpreted in terms of gravity (GW) or Rossby waves (RW)
25 that are identified with vertical and quasi-horizontal displacements, respectively. Using the
26 method of *Pierce and Grant* [1998] as applied by *Thompson et al.* [2007a,b], amplitudes and
27 frequencies in ozone laminae are compared among representative SHADOZ sites over Africa
28 and the Pacific, Indian and Atlantic Oceans. GW signals maximize in the TTL and lower
29 stratosphere. Depending on site and season, GW is identified in up to 90% of the soundings.
30 GW are most prevalent over the Pacific and eastern Indian Oceans, a distribution consistent
31 with vertically propagating equatorial Kelvin waves. Ozone laminae from RW occur more
32 often below the tropical tropopause and with lower frequency (< 20%). Gravity Wave and
33 Rossby Wave Indices (GWI, RWI) are formulated to facilitate quantitative comparison of
34 wave signatures among sites and analysis of interannual variability. GWI is positively
35 correlated with a standard ENSO (El-Niño-Southern Oscillation) index over American
36 Samoa (14°S, 171°W) and negatively correlated at Watukosek, Java (7.5°S, 114°E), Kuala
37 Lumpur (3°N, 102°E) and Ascension Island (8°S, 15°W). GWI and RWI are positively
38 correlated with the Quasi-Biennial Oscillation at Natal, Brazil (6°S, 35°W).

39 **1. Introduction**

40 **1.1 Prior Work and Overview of Study**

41 Wave activity in the tropics plays a role in transporting ozone and water vapor in the
42 upper troposphere and lower stratosphere (UT/LS), thus contributing to circulation,
43 radiative and dehydration processes in this region. Analysis of waves in the tropical UT/LS

44 sheds insight on the ongoing discussion about the relative contributions of regional
45 upwelling, advection, and overshooting convection to the transport of constituents from
46 troposphere to stratosphere. For instance, when convection in the tropical troposphere
47 initiates a Kelvin wave (a type of gravity wave), a transient deformation of the tropopause
48 takes place, often with descent of colder, higher-ozone air into the UT [*Fujiwara et al.*, 1998;
49 *Fujiwara and Takahashi*, 2001; *Fujiwara et al.*, 2003a; 2009]. It has also been suggested that
50 tropical Rossby waves can drive a forced ascent over the equatorial UT/LS, providing a
51 mechanism for carrying moist tropospheric air into the stratosphere [*Boehm and Lee*, 2003;
52 *Ryu and Lee*, 2009].

53 Vertically propagating equatorial Kelvin waves not only contribute to constituent
54 transport, but they play an important role for driving tropical tropopause undulations at
55 intraseasonal time scales [*Zhou and Holton*, 2002; *Son and Lee*, 2007; *Suzuki and Shiotani*,
56 2008; *Ryu et al.*, 2008 [RLS, hereafter]]. Kelvin waves may be involved in dehydrating
57 tropospheric air that enters the stratosphere [*Tsuda et al.*, 1994; *Randel and Wu*, 2005; RLS;
58 *Ryu and Lee*, 2009]. As such, an objective analysis of the tropical Kelvin and Rossby wave
59 climatology will enhance our understanding of physical processes affecting the variability of
60 tropical stratosphere-troposphere exchange.

61 One approach to characterizing tropical wave activity is to examine the evidence of
62 dispersion relations of the waves using proxy observations [*Wheeler and Kiladis*, 1999;
63 *Roundy and Frank*, 2004a,b; *Kiladis et al.*, 2009]. While this is useful in bridging a gap
64 between theory and observations, it does not provide regionally dependent wave
65 characteristics. The present study uses the zonally distributed SHADOZ soundings
66 [*Thompson et al.*, 2003a,b] with the laminar formalism [*Teitelbaum et al.*, 1994; 1996; *Pierce*
67 *and Grant*, 1998; *Thompson et al.*, 2007a,b] to examine the extent to which this approach can
68 identify and quantify certain types of tropical waves. A successful outcome would produce a
69 regional wave climatology that serves as a reference for studies of tropical composition and

70 dynamics in a changing climate (*Gettelman and Birner, 2007; Garcia and Randel, 2008;*
71 *Gettelman and Hegglin, 2009; Gettelman et al., 2009*).

72 In the first application of the laminar method to tropical sonde data, *Grant et al. [1998]*
73 analyzed the longest record at that time, 1979-1993 at Natal, Brazil (6°S, 35°W), and shorter
74 sets of sounding from Africa, Ascension Island (8°S, 14°W) and Samoa (14°S, 171°W). *Grant et*
75 *al. [1998]* found that Rossby-waves (RW), used to represent horizontal displacements of air
76 parcels, were less frequent than so-called gravity waves (GW), the designation for ozone
77 layers associated with vertical motions. The latter appeared regularly in the LS and in the
78 region designated as the tropical tropopause layer (TTL), the transition zone between 14 and
79 18.5 km (150-70 hPa; *Dessler, 2002; Folkins et al., 2002; Gettelman and Forster, 2002; Yang et*
80 *al., 2008; Fueglistaler et al., 2009*).

81 A second tropical study using laminar identification (LID in *Thompson et al. [2009]*)
82 presented wave statistics based on soundings taken over Heredia, Costa Rica (10°N, 84°W)
83 and Panamá (7.8°N, 80°W) during the 2007 TC4 campaign (Tropical Composition, Cloud and
84 Climate Coupling; *Toon et al., 2009*). The GW and RW frequency and distribution at these
85 central American sites are similar to those inferred from SHADOZ soundings at San Cristóbal
86 (1°S, 90°W) and Paramaribo (5°N, 55°W). Kelvin waves were reported over San Cristóbal
87 [*Fujiwara et al., 2001*] and Paramaribo [*Immler et al., 2008*].

88 **1.2 Road Map of Study**

89 Almost none of the stations mentioned above is located in the Indian Ocean or western
90 Pacific where convectively driven Kelvin waves are most active [*Randel and Wu 2005; RLS*].
91 The ten-year SHADOZ dataset offers a well-resolved (50-100 m in vertical), accurate (~5%;
92 *Thompson et al., 2007c*) ensemble of profiles from a dozen tropical and subtropical zonally
93 distributed sites, including the western Pacific. The laminar technique is applied
94 systematically to the SHADOZ data to characterize regional climatology and variability of

95 tropical Rossby and Kelvin wave signatures, using the GW designation as a proxy for the
96 latter. We address the following questions:

- 97 ▶ What are seasonal and interannual signatures of convection in ozone?
- 98 ▶ Where do these features occur geographically?
- 99 ▶ Are convective and wave patterns based on ozone variations consistent with prior
100 studies of these influences, particularly over the Pacific and eastern Indian Oceans?
- 101 ▶ What is the structure of ozone within the UT-LS inferred from soundings?
- 102 ▶ Given that the laminar formalism points to ubiquitous signatures of GW in the UT-LS,
103 what are differences in seasonal and interannual variations at each site?

104 We also construct indices based on GW and RW frequency to look for signals related to the
105 two prominent sources of interannual variability, El Niño-Southern Oscillation (ENSO) and
106 | Quasi-Biennial Oscillation (QBO). Data and analytical methods are described in **Section 2.**
107 | **Section 3** presents ozone structure in the free troposphere (FT), TTL and LS, characteristics
108 | of RW and GW waves at representative SHADOZ sites and the RW and GW Indices. **Section 4**
109 is a Summary.

110 **2. SHADOZ Observations and Methods of Analysis**

111 **2.1 Data: 1998-2007**

112 The SHADOZ network has collected > 4000 profiles from over 14 stations from 1998-
113 2007 [*Thompson et al., 2003a,b*]. Ozone and temperature data used in this study were
114 reprocessed in April 2007; selected profiles were corrected or discarded (<5% of total)
115 relative to data used earlier (e.g. *Thompson et al., 2003a,b; Folkins et al., 2006; Fu et al., 2007*).

116 | **Table 1** presents location of sites used in this study with years of record and numbers
117 of soundings contributing. The ozone measurement is made with electro-chemical
118 concentration cell ozonesondes [*Johnson et al., 2002; Thompson et al., 2000; 2003a*].

119 Temperature, pressure, humidity are recorded by standard radiosondes launched with each

120 ozonesonde. Vaisala RS-80 or RS-92 radiosondes are used at all stations except Ascension
121 and Natal, as described at <<http://croc.gsfc.nasa.gov/shadoz>>. With standard protocols
122 employed at the SHADOZ sites [Smit *et al.*, 2009], the precision of the ozone measurement is
123 5%. Accuracy of the ozone reading below 20 km is also 5% [Thompson *et al.*, 2003a; 2007c].
124 Slight variations in sonde solution as well as different instrument types [Smit *et al.*, 2007;
125 Deshler *et al.*, 2008] can introduce biases in absolute ozone readings among individual
126 SHADOZ sites (Figure 9 in Thompson *et al.*, 2003a; Figure 8 in Thompson *et al.*, 2007c). They
127 do not affect wave identification here, where laminae (Section 2.2) unique to each sounding
128 are used [Pierce and Grant, 1998; Thompson *et al.*, 2007a,b].

129 2.2 Laminar Identification (LID) Method for Wave Detection

130 The technique described in Pierce and Grant [1998], adapted from Teitelbaum *et al.*
131 [1994], is used to isolate laminae and to determine wave-type origins. The steps below refer
132 to **Figure 1**. Archived SHADOZ data contain relative humidity (plotted to ~ 200 hPa in
133 Supplementary Material, **Figure S-1**), ozone partial pressure and temperature (left panel,
134 **Figure 1a**) and in ozone mixing ratio (right panel, **Figure 1a**).

135 Step 1: For each sounding, we locate laminae in O_3 and potential temperature, θ , through
136 normalization to running means over altitude. A boxcar smoothing over 2.5 km is
137 used to isolate each lamina. Larger and smaller ranges have been tested with little
138 difference in laminar statistics. Results for one profile are illustrated in **Figure 1b**,
139 where normalized O_3 is the solid line; the θ deviations are signified by the dotted line.
140 Because the ozone mixing ratio precision is 5%, only laminae representing a deviation
141 of $\geq 10\%$ (red vertical lines in **Figure 1b**) are included in the analysis. Note that O_3
142 deviations often exceed 20% in the TTL (generally defined as 14-18.5 km) and LS to ~
143 20 km. The θ variations are relatively small below 15 km (cf Noguchi *et al.*, 2006). The
144 patterns in **Figure 1b** over Fiji are typical of SHADOZ sites.

145 Step 2: Correlations between O_3 and θ gradients are used to identify GW and RW. The
146 correlation (dashed line in **Figure 1b**), with positive values > 0.7 defines GW (light
147 green in **Figure 1b**), based on the reasoning that the correlation between the two
148 quantities signifies a vertical disturbance. Conversely, when horizontal motion affects
149 O_3 , it is poorly correlated with θ . The standard practice of *Pierce and Grant* [1998] and
150 *Teitelbaum et al.* [1994], sets the RW limit for anti-correlation at ± 0.3 , corresponding
151 | to light blue sections in **Figure 1b**. The criterion employed here, i.e. only O_3 laminae
152 reaching a 10% deviation are assigned RW or GW identity, limits the range of wave-
153 | labeled segments to the darker green and blue levels (**Figure 1b**).

154 Step 3: Summary statistics are computed for each site. First is the amplitude of laminae, as
155 % of the local deviation. The second parameter is frequency, defined as percent of the
156 number of soundings in which the given wave type appears, determined at $\frac{1}{2}$ km
157 intervals. A third parameter, an ozone budget, is produced by adding column-
158 integrated O_3 amounts within each layer designated as GW or RW, typically for the
159 troposphere or to 20 km [*Thompson et al.*, 2009].

160 **2.3 Statistics of Wave Variability at Selected SHADOZ Sites**

161 Indices for wave activity are used to evaluate interannual variability. The RW and GW
162 Indices (RWI and GWI) are based on the fraction of the column (up to 20 km) included in RW
163 | or GW laminae that meet the 10% deviation criterion (dark blue and green layers in **Figure**
164 | **1b**). The GWI and RWI are normalized prior to correlation analysis with ENSO and QBO
165 indices. The Bivariate ENSO Time-series (BEST) is used to represent ENSO [*Smith and*
166 *Sardeshmukh*, 2000]; the QBO index is obtained from the zonal average of the 30hPa zonal
167 wind at the equator <<http://www.esrl.noaa.gov/psd/data/ /climateindices/list/>>. A two-
168 sided test is used to determine statistical significance.

169 **3. Results and Discussion**

170 **3.1 Ozone Climatology. Time - Series and Seasonality**

171 Ozone mixing ratios are presented first as time-series throughout the troposphere and
172 TTL with a close-up of TTL and LS ozone available in Supplementary Material.

173 3.1.1 Tropospheric and TTL Ozone (1998-2007)

174 A summary of ozone mixing ratio curtains during 1998-2007 for representative
175 SHADOZ sites appears in **Figure 2**. Seasonal and interannual variability is evident at each
176 location. For example, green-yellow-orange shading in the 4-11 km region may signify long-
177 distance transport of persistent pollution from biomass fires [*Thompson, 2004*], a process
178 with a roughly annual cycle at most sites. At La Réunion, Natal, and Ascension (**Figures**
179 **2b,g,h**), ozone from advection and in-situ formation are often stronger than over Nairobi,
180 Samoa and San Cristóbal (**Figures 2a,e,f**). For Natal and Ascension (**Figures 2g,h**), as over
181 the tropical Atlantic in general, long-range transport of mid-tropospheric O₃, as well as O₃
182 from convective mixing [*Kley et al., 2007*] of surface O₃ precursors (hydrocarbons, CO, NO),
183 and lightning-derived NO [*Jenkins et al, 2003; Jenkins and Ryu, 2004*] are recorded in satellite
184 data [*Fishman et al., 1996; Thompson et al., 2000; Edwards et al., 2003*]. Relative amounts of
185 advected O₃ [*Thompson et al., 1996*], stratospheric subsidence [*Krishnamurti et al., 1996*] and
186 photochemistry [*Jacob et al., 1996*] over the south tropical Atlantic during austral spring
187 were deduced from sondes and aircraft data taken in the 1992 SAFARI/TRACE-A campaign.
188 The greatest tropospheric O₃ formation occurs near African sources (Figure 15 in *Thompson*
189 *et al., 1996*; also *Thompson et al., 2002*). Ozone formation in the UT varies with background
190 levels of NO (1-2 ppbv O₃/day net formation; *Smyth et al. 1996*) or lightning-enhanced NO
191 (10-15 ppbv O₃/day; *Pickering et al., 1996*; cf *Morris et al., 2009*).

192 Ozone structure over La Réunion (**Figure 2b**) reflects a mixture of subsidence,
193 entrainment of extra-tropical air and convection over the Indian Ocean. This has been
194 observed in satellite tropospheric O₃ data [*Chatfield et al., 2004; 2007*] and in sonde-lidar
195 observations [*Randriambelo et al., 2003; Clain et al., 2009*]. Stratospheric influences, in
196 downward transport, or as filaments from the extra-tropics are frequent at La Réunion

197 [Baray et al., 1998; 1999; Le Claire du Bellevue et al., 2006] and over Irene [Diab et al., 1996;
198 2004] and to a lesser degree, over San Cristóbal [Fujiwara et al., 2001].

199 | Over the eastern Indian Ocean, Watukosek and Kuala Lumpur (**Figures 2c,d**) display
200 lower ozone than Nairobi and La Réunion, and Atlantic sites. A sharper ozone gradient and
201 | higher altitude characterize the TTL. Over the Pacific (Samoa and San Cristóbal, **Figures**
202 | **2e,f**), mid-tropospheric O₃ maxima are due to long-range pollution transport [Oltmans et al.,
203 2001], although this feature may vary with the El Niño-La Niña cycle [Lee et al., 2009] i.e.
204 alternating effects of subsidence or convection. ENSO-induced drought may contribute to
205 pollution, as during the 1997-1998 [Fujiwara et al., 1999; Thompson et al., 2001] and 2006
206 Indonesian biomass fires [Logan et al., 2008]. In other regions, an ENSO can suppress fire
207 activity and ozone [Thompson and Hudson, 1999].

208 | Similar features to those at San Cristóbal (**Figure 2f**) were observed in sondes over
209 Christmas Island (1.5° N, 157°W) in the central Pacific [Takashima et al., 2008]. Context for
210 TTL over San Cristóbal is provided by the TC4 soundings taken in July-August 2007 over
211 Costa Rica and Panamá (Figure 2 in Thompson et al., 2009).

212 In addition to ozonopause variability among SHADOZ sites, temperature and relative
213 | humidity also vary (**Supplementary Figure S-1**; for details, see Loucks, 2007). Kuala
214 Lumpur is wettest up to the TTL, fairly evenly over the year, although biases among humidity
215 sensors used in SHADOZ caution against quantitative interpretation.

216 3.1.2 Tropospheric Ozone Seasonality (mean)

217 | **Figure 3** highlights seasonality of representative SHADOZ sites in monthly mean
218 ozone contours. The most distinctive variations among sites occur in: (a) the FT-TTL
219 transition; (b) signatures of convection, in which low-O₃ BL air is directed up to mid- and
220 | upper troposphere; (c) timing and location of pollution impacts. In **Figure 3a**, Nairobi shows
221 a gradual transition from FT to TTL, from ~70 ppbv to 125 ppbv (yellow-to-red) suggestive
222 of a descending branch of the Walker circulation. Because Nairobi straddles the Intertropical

223 Convergence Zone (ITCZ), this pattern is twice-yearly, in April-May at the end of the northern
224 tropical wet season, and in September-December.

225 Convective signatures are evident when low-O₃ BL air, typically over the ocean, is
226 directed upward into the mid-upper troposphere. This occurs in February-March and July-
227 August over Watukosek (**Figures 3b**) and Kuala Lumpur from July to September and again in
228 December-February (**Figure 3c**). Surface and mid-upper tropospheric low-O₃ air may be
229 separated by a layer of higher O₃, as in May over Watukosek and Samoa (**Figures 3b,d**) and
230 during January and February over San Cristóbal and Natal (**Figure 3e,f**). Although mid-
231 tropospheric, high-O₃ layers normally maximize in the latter part of the year, i.e. during the
232 southern hemisphere fire season (August to November, **Figures 3a,d-f**), a secondary mid-
233 troposphere O₃ maximum appears over Nairobi in May-July (**Figure 3a**) and Natal in January-
234 March (**Figure 3f**), possibly due to cross-ITCZ fire pollution. *Thouret et al.* [2009] discuss the
235 complexity of the two-year Cotonou SHADOZ record with respect to fire impacts crossing the
236 equator.

237 Although we focus principally on the FT and TTL, the BL shows significant features at
238 certain locations (**Figures 2 and 3**). With the exceptions of Watukosek (**Figures 2c and 3b**),
239 Irene and Paramaribo (not shown), BL pollution is unusual at SHADOZ sites. A roughly
240 annual cycle in BL ozone follows lower FT ozone over La Réunion (**Figure 2b**). The mid-
241 troposphere O₃ maximum (4-11 km) occurs in the October-March period, sometimes more
242 skewed toward September-October -November (1998, 1999, 2004, 2006, 2007) and other
243 times, in December, January-to-March (2000-2001; 2001-2002; early 2003). Distinctive FT-
244 BL connections during elevated ozone periods occur over Natal (**Figures 2g and 3f**) and
245 Ascension (**Figure 2h**). The maximum linkage may occur toward the early wet season
246 (November-to-January), as in 1999-2000 or mid-year as in 2001 and 2005. Ascension and
247 Natal patterns are alike but the BL height is lower and less variable at Ascension and the
248 signature of FT subsidence more profound. This leads to a zonal wave-one structure

249 | [Shiotani, 1992; Thompson et al., 2003b]. Signatures of convection are less frequent at
250 | Ascension (cf mid-troposphere above Ascension, < 35 ppbv O₃; blue color in **Figure 2h**) than
251 | at Natal (**Figures 2g and 3f**).

252 | 3.1.3 TTL-LS Ozone and Seasonality

253 | Analyses of TTL height and thickness, averaged over SHADOZ sites, have been
254 | presented by *Randel et al* (2007; see Figures 2 and 3), *Fu et al.* [2007] and *Konopka et al.*
255 | [2009]. Station-to-station annual patterns were characterized by *Takashima and Shiotani*
256 | [2007]. Annual cycles in tropopause height and structure of the TTL (14-18 km) and LS are
257 | captured in **Figure S-2**. An exceptionally low TTL, as indicated in the red-to-brown
258 | transition, appears over Watukosek and Kuala Lumpur in 1998-1999 (**Figure S-2b,c**) during
259 | the strong 1997 ENSO and Indian Ocean Dipole [*Thompson et al.*, 2001]. During that period a
260 | higher-than-normal TTL, induced by more active convection, appeared over Nairobi and San
261 | Cristóbal, and somewhat over Ascension (**Figure S-2a, f, h**). A similar pattern occurred as an
262 | ENSO develops from 2005 to 2006.

263 | **3.2 Wave Characteristics**

264 | 3.2.1 Seasonality at Representative SHADOZ Sites

265 | **Figure 4** illustrates monthly averaged laminae amplitude for five sites. Amplitudes
266 | are in the 12-20% range with the magnitude distributed fairly evenly with altitude and over
267 | the course of the year. There are mid-tropospheric laminae at several periods throughout the
268 | year that may signify long-range pollution; see localized maxima in **Figure 3**. These occur in
269 | September over Nairobi and Samoa (**Figure 4a,c**), November (Watukosek, **Figure 4b**), and in
270 | October-November, when African and South American pollution intermingle over Natal
271 | (**Figure 4e**). Pronounced maxima in amplitude are found at ~10 km during the wet season
272 | (February-March-April) over Watukosek (**Figure 4b**) and at 13 km over Natal (**Figure 4e**).
273 | At all sites except Kuala Lumpur (**Figure 4c**), the amplitude of TTL laminae increases ~15%
274 | in September-October-November.

3.2.2 Site-to-site Variations in GW/RW

The frequency of wave occurrence over altitude and annual cycle is depicted in **Figures 5 and 6**, for GW and RW, respectively. Shading indicates statistical significance. There appear to be two sets of GW frequency maxima with distinct altitude and seasonality. One set of GW maxima appears at the TTL-LS interface with roughly quarterly periodicity. A good example is at Nairobi (**Figure 5a**) where the maximum is centered at 17.5-18.5 km, nominally in the LS, in late January-February, 1 May, 15 July, 1 November. A separate feature in the lower TTL (~14-15 km) appears in mid-January and in the mid-July to September period, ie roughly semi-annually (**Figure 5**). Aspects of TTL seasonality have been detailed by *Takashima and Shiotani* [2007]; *Randel et al.* (2007); *Konopka et al.* [2009]. *Folkins et al.* [2006], using western Pacific/eastern Indian Ocean SHADOZ data in the TTL, showed convective impacts minimizing in June and maximizing in DJF.

RW occurrence is less prominent in the TTL but still relatively high (10% or more) over Nairobi, Watukosek and Samoa (**Figure 6a,b,d**). Near-surface RW frequency >20% at Kuala Lumpur may denote advection of regional pollution [*Yonemura et al.*, 2002]. Mid-tropospheric RW activity is greatest in September-October, 35% over Nairobi and Watukosek (**Figure 6a,b**), and 10-15% over Natal (**Figure 6e**). For Natal (cf **Figure 2f**), these levels correspond to advection of African pollution [*Logan and Kirchhoff*, 1986; *Thompson et al.*, 1996]. Above 8-10 km, the RW may signify pollution plumes from South American fires [*Fishman et al.*, 1996; *Pickering et al.*, 1996]. Relatively high GW and RW frequencies both occur in September-October over Natal (**Figure 5e**); impacts of early wet-season convection and late-fire season pollution may coincide [*Thompson et al.*, 1997].

Averaging the GW and RW frequencies over the year (**Figure 7**) highlights regional differences. The GW frequency is greater closer to the equator and RW frequency increases with latitude (**Figure 7**). Sub-tropical Réunion and Irene (distinct profile shape relative to sites equatorward of 15°S, *Thompson et al.*, 2007c) have the lowest mean GW frequency,

301 | ~20% (**Figure 7a**). Likewise, the GW frequency (**Figure 7a**) over Fiji (40%; latitude, 18°S) is
302 | lower than over San Cristobal (1°S), Kuala Lumpur (3°N) or Watukosek (7.5°S). The Indian
303 | Ocean and Pacific sites have higher GW frequencies than the Atlantic stations, approximately
304 | a factor of two on average (**Figure 7a**). The GW frequency peaks at 50-75% over Nairobi and
305 | Malindi, in a western Indian Ocean meteorological regime, and over Kuala Lumpur and
306 | Watukosek, eastern Indian Ocean stations within +/-10 degrees latitude. Atlantic sites within
307 | 8 degrees latitude have a GW frequency at 40%.

308 | Paramaribo GW frequency and seasonality (Figure 5 in *Thompson et al., 2009*) are
309 | similar to those for Natal (**Figure 7a**). Intensive soundings at the Costa Rican SHADOZ site
310 | (initiated in 2005) and over southwestern Panamá during TC4 revealed robust GW activity in
311 | the TTL (Figures 1 and 4 in *Thompson et al., 2009*). Also in TC4, temperature soundings taken
312 | four times daily detected convectively generated waves [*Selkirk et al., 2009*]. Convective
313 | impacts in layers ~1 km thick were confirmed with aircraft tracers [*Avery et al., 2009*;
314 | *Petropavlovskikh et al., 2009*].

315 | RW are prominent in the mid-to-lower troposphere, but overall occurrence is less
316 | frequent than for GW (note scale difference, maximum < 30%, **Figure 7b**). Elevated RW in
317 | the TTL is expected at sites farther from the equator in austral spring, when stratospheric
318 | influence increases, ie, over La Réunion (21°S; *Baray et al., 1998; 2003; Portafaix et al., 2003*;
319 | *Randriambelo et al., 2003*) and Irene (26°S; *Diab et al., 1996; Thompson et al., 1996*).

320 | Seasonal and longitudinal patterns of wave frequency appear as a composite in **Figure**
321 | **8**. **Figure 8a** displays GW frequency based on averaging over 15-20 km (~60-125 hPa). The
322 | average of the RW frequency below 100 hPa (cf **Figure 7b**) is used for **Figure 8b**. The
323 | minimum GW frequency occurs over the highest latitude sites (Réunion, Irene) and the
324 | Atlantic (e.g. Ascension, **Figure 8a**). Moderately high GW frequencies are found over the
325 | Pacific (Fiji, Samoa, San Cristobal). The RW structure is less distinct; the maximum value in
326 | **Figure 8b** is about ¼ that in **Figure 8a**.

3.3 Indices for Wave Impact: GWI and RWI

The Gravity and Rossby Wave Indices (**Figure 9**; additional sites in Supplemental **Figure S-3**) suggest that GWI and RWI are inversely related; if laminae are present, one or the other wave type is identified. The general pattern of greater GW activity over the western Pacific and eastern Indian Oceans (**Figures 7 and 8**) holds, ie higher GWI at those sites (**Table 2**). For example, the mean GWI over Nairobi, Watukosek and Kuala Lumpur (**Figures 9a-c**) is ~15% although the range of GWI at these sites varies greatly. At Nairobi and Watukosek (**Figures 9a,b**) GWI ranges from 5-20% but at Kuala Lumpur, except for 1998, the range is 10-20%. The 1998 Watukosek and Kuala Lumpur anomalies are consistent with the strong ENSO. Reduced GWI in early 1998 is presumably due to suppressed convection, followed by sharp increases in 1999 when the La Niña gathered strength. In Nairobi GWI was at a high point in early 1998 but by mid-1998 it had fallen to its lowest value in the 1998-2007 period. In 2006 a fairly strong ENSO occurred (cf *Logan et al.* 2008), signified by a Nairobi GWI maximum (**Figure 9a**; mean GWI in **Table 2**) and a decline in the Kuala Lumpur GWI; over Watukosek data gaps confuse patterns after 2005. At Samoa (**Figure 9d**) the 1997 ENSO led to a GWI maximum, followed by an 18-point (absolute) decline; the Fiji record (**Figure S-3a**) is similar. Natal (**Figure 9e**) soundings were sparse in 1998. Ascension (refer to **Figure S-3b**) began with a high GWI in 1998 that declined rapidly. In general Ascension has a greater GWI range than Natal (**Figure 9e**) although the annually averaged GW frequency and structure is nearly the same at the two sites. The GWI at Paramaribo at (5°N, Figure 13 in *Thompson et al.*, 2009; **Table 2** here) is slightly less than the Natal GWI at 5.5°S. Irene and La Réunion typically display GWI < 10% (**Figures S-3c,d**). At Irene GWI was at a 9-year maximum in 1999 due to the La Niña. We have investigated the possibility of trends in GWI and RWI over the 1998-2007 period, but the record is too short to be useful.

In **Table 2** GWI and RWI, monthly averaged, are related to the ENSO and QBO, with statistically significant correlations indicated by red letters. The clearest ENSO signals are for

353 | Kuala Lumpur and Samoa (**Figures 9c,e**), with positive GWI correlation in the latter (more
354 convection in the Pacific) and negative for the former (suppressed convection in the eastern
355 Indian Ocean). The correlation between GWI and ENSO over Watukosek is similar to that for
356 | Kuala Lumpur but not statistically significant. Positive RWI relationships with ENSO (**Table**
357 | **2**) may reflect subsidence over Kuala Lumpur (**Figure 9c**) and/or transport of pollution from
358 Indonesian fires [*Fujiwara et al.*, 1999; *Oltmans et al.*, 2001; *Thompson et al.*, 2001; *Yonemura*
359 *et al.*, 2002].

360 *Randel et al.* [2009] examined the relationship in zonally averaged LS temperature and
361 ozone with a chemical-climate model and SAGE (Stratospheric Aerosol and Gas Experiment)
362 data. In regressions with a multi-variate ENSO index, negative ozone anomalies from 15-20
363 km were detected in the satellite data and the model. This would be consistent with a
364 | reduced GWI (negative signals in **Table 2**). However, the present results, as well as the
365 detailed profile analysis of *Lee et al.* [2009] argue that regional and vertical variations due to
366 ENSO and QBO impacts (cf *Logan et al.*, 2003; *Witte et al.*, 2008) are masked by zonal
367 averaging.

368 **4. Summary**

369 The ten-year SHADOZ record (1998-2007) has been used to study variability in the
370 troposphere, TTL and LS (surface to 20 km). Vertical structure is examined across seasons
371 and regionally with two sites each in the Pacific (Samoa, San Cristóbal) and Atlantic (Natal,
372 Ascension), two in Africa (Nairobi, Irene) and three in the Indian Ocean (La Réunion,
373 Watukosek, Kuala Lumpur). Addressing questions about variability in ozone vertical
374 structure in the FT and TTL, we find:

375 1) At each site, ozone mean mixing ratios and time-series variations over the ten-
376 year period are distinct. In the FT, mixing ratios as low as 10 ppbv, presumably due to
377 convection from the BL, are prominent over Kuala Lumpur, Watukosek, Samoa and Fiji. In

378 contrast, over Natal, Ascension and La Réunion, FT ozone maxima are typically associated
379 with biomass burning.

380 2) The seasonality of convection, as manifest in FT O₃, also varies site-to-site. At
381 all SHADOZ stations, the most consistent convective activity, in D-J-F, coincides with a
382 maximum in GW frequency. Secondary periods of intense convection in occur May-July over
383 Samoa, Watukosek, Natal and Nairobi.

384 3) TTL thickness, as measured by ozone gradient, and the TTL-FT transition also
385 vary site-to-site. Generally, sites near descending branches of the Walker circulation display
386 a more gradual transition (e.g. Nairobi, Natal, Ascension). Regions of ascent (Watukosek,
387 Kuala Lumpur) have a sharper transition and a higher altitude for the TTL.

388 4) Pollution and/or stratospheric influences are signified as recurrent ozone
389 maxima (> 100 ppbv in individual soundings, > 70 ppbv as monthly averages) in the FT,
390 mostly in the 4-12 km range. These features tend to dominate August-December, except at
391 Kuala Lumpur (opposite seasonality; it is north of the ITCZ; *Yonemura et al., 2002*).

392 We made a systematic application of the laminar method to identify RW and GW
393 activity over the 1998-2007 period. RW activity, appearing in fewer than 20% of SHADOZ
394 soundings, appears to be of two types. RW is often associated with intrusions of extra-
395 tropical air, especially in austral spring. This occurs at sub-tropical sites, e.g. La Réunion
396 [*Clain et al., 2009*], but also at more equatorial locations, e.g., Christmas Island [*Takashima et*
397 *al., 2008*]; Indonesia [*Fujiwara et al., 2003b*]; Paramaribo, Costa Rica [*Thompson et al., 2009*].
398 Second, RW may represent pollution, either local (Kuala Lumpur, Watukosek) or in stable
399 layers transported thousands of km (Samoa, San Cristóbal, Natal).

400 Signatures of gravity waves in the TTL and LS are a semi-permanent feature at all
401 SHADOZ sites, detected in 50% of the soundings. GW frequency is greatest near the top of the
402 TTL, ~18 km, in D-J-F and a minimum in June and July. GW activity is presumed to signify
403 Kelvin waves initiated by convection. The amplitude of laminae (10-20%) is similar among

404 all SHADOZ sites. GW frequency is > 40% at all sites equatorward of 20°S and two times
405 greater at several equatorial locations than at La Réunion and Irene.

406 Interannual variability in GW and RW activity was studied with Indices that also
407 quantify regional differences. A study of factors influencing GWI and RWI was made through
408 comparison with standard ENSO and QBO indices. For sites with the highest GWI (Kuala
409 Lumpur and Watukosek) that register a significant anti-correlation with ENSO, and a positive
410 RWI correlation, suppressed convection is a plausible explanation. Both GWI and RWI are
411 positively correlated with the QBO over Natal.

412 An important consequence of regional GW and RW variations is a caution against
413 over-averaging among SHADOZ sites. *Lehmann and Rex* [2008] reached similar conclusions
414 regarding inferred rates of vertical ascent in the TTL and LS. Regional differences in Kelvin
415 wave properties at the TTL are described in *Suzuki and Shiotani* [2009]. *Lee et al.* [2009]
416 have performed EOF (Empirical Orthogonal Function) analysis on SHADOZ ozone anomalies
417 between 17 and 30 km and used the resulting principal components of the first two EOFs as
418 indices for the QBO. Results of their ozone and temperature analysis based on these indices
419 show strong regional variations in the troposphere due to both QBO and ENSO.

420 **Acknowledgments.** This research is based on the MS thesis of A. Loucks (Allen) and was
421 supported by NASA Grants NNG05GP22G and NNX09AJ23G (thanks to M. J. Kurylo, K. W. Jucks). We
422 are grateful for comments by M. Fujiwara (Hokkaido Univ), A. E. Dessler (Texas A and M Univ), J-L
423 Baray and S. Venkataraman (Univ Réunion).

424 **References.**

425 Avery, M. A., et al. (2009), Convective distribution of tropospheric ozone and tracers in the
426 central American ITCZ region: Evidence from observations during TC4, *J. Geophys.*
427 *Res.*, to be submitted.

428 Baray, J. L., G. Ancellet, F. G. Taupin, M. Bessafi, S. Baldy, and P. Keckhut (1998), Subtropical
429 tropopause break as a possible stratospheric source of ozone in the tropical
430 troposphere, *J. Atmos. Sol.-Terr. Phys.*, **1** (60), 27–36.

431 Baray J. L., G. Ancellet, T. Randriambelo, and S. Baldy (1999), Tropical cyclone Marlene and
432 stratosphere-troposphere exchange, *J. Geophys. Res.*, **104**(D11), 13953–13970.

433 Baray, J-L, S. Baldy, R. D. Diab, and J-P Cammas (2003), Dynamical study of a tropical cut-off
434 low over South Africa and its impact on tropospheric ozone, *Atmos. Environ.*, **37**, **11**,
435 1475-1488.

436 Boehm, M., and S. Lee (2003), The implications of tropical Rossby Waves for tropical
437 tropopause cirrus formation and for the equatorial upwelling of the Brewer–Dobson
438 circulation, *J. Atmos. Sci.*, **60**, 247–261.

439 Clain, G., J-L Baray, R. Delmas, R. Diab, J. Leclair de Bellevue, P. Keckhut, F. Posny, J. M. Metzger,
440 and J. P. Cammas (2009), Tropospheric ozone climatology at two Southern
441 Hemisphere tropical/subtropical sites, (Reunion Island and Irene, South Africa) from
442 ozonesondes, LIDAR, and in situ aircraft measurements, *Atmos. Chem. Phys.*, **9**,
443 1723–1734.

444 Chatfield, R. B., H. Guan, A. M. Thompson, J. C. Witte (2004), Convective lofting links Indian
445 Ocean air pollution to paradoxical south Atlantic Ozone Maxima, *Geophys. Res. Lett.*, **31**,
446 L06103, doi: 10.1029/2003GL018866.

447 Chatfield, H. Guan, A. M. Thompson, H. G. J. Smit (2007), Mechanisms for the intraseasonal
448 variability of tropospheric ozone during the Indian winter monsoon, *J. Geophys. Res.*,
449 **112**. D10303, doi: 10.1029/2006JD007347.

450 Deshler, T., et al. (2008), Balloon Experiment to test ECC-ozonesondes from different manu-
451 facturers, and with different cathode solution strengths: Results of the BESOS flight, *J.*
452 *Geophys. Res.*, **113**, D04307, doi:10.1029/2007JD008975.

453 Dessler, A. (2002), The effect of deep, tropical convection on the tropical tropopause layer, *J.*
454 *Geophys. Res.*, **107**, 4033, doi: 10.1029/2001JD000511.

455 Diab, R. D., et al. (1996), Vertical ozone distribution over southern Africa and adjacent oceans
456 during SAFARI-92, *J. Geophys. Res.*, **101**, 23,809-23,821.

457 Diab, R. D., A. M. Thompson, K. Mari, L. Ramsay, and G. J. R. Coetzee (2004), Tropospheric
458 ozone climatology over Irene, South Africa from 1990-1994 and 1998-2002, *J. Geophys.*
459 *Res.*, 109, D20, D20301, doi: 10.1029/2004JD004293.

460 Edwards, D., et al., (2003), Tropospheric ozone over the tropical Atlantic: A satellite
461 perspective, *J. Geophys. Res.*, **108**, 4237, doi: 10.1029/2002JD002927.

462 Fishman, J., V. G. Brackett, E. V. Browell, and W. B. Grant (1996) Tropospheric ozone derived
463 from TOMS/SBUV measurements during TRACE-A, *J. Geophys. Res.*, **101**, 24069-
464 24082.

465 Folkins, I., C. Braun, A. M. Thompson, J. C. Witte (2002). Tropical ozone as an indicator of deep
466 convective outflow, *J. Geophys. Res.*, 107, D13, doi: 10.1029/2001JD001178.

467 Folkins, I., P. Bernath, C. Boone, K. Walker, A. M. Thompson, J. C. Witte (2006) The seasonal
468 cycles of O₃, CO and convective outflow at the tropical tropopause, *Geophys. Res. Lett.*,
469 **33**, L16802, doi: 10.1029/2006GL026602.

470 Fu, Q., Y. X. Hu and Q. Yang (2007), Identifying the top of the tropical tropopause layer from
471 vertical mass flux analysis and CALIPSO lidar cloud observations, *Geophys. Res. Lett.*,
472 **34**, L14813, doi:10.1029/2007GL030099.

473 Fueglistaler, S., A. E. Dessler, T. J. Dunkerton, I. Folkins, Q. Fu, and P. W. Mote (2009) The
474 tropical tropopause layer, *Rev. Geophys.*, 47, RG1004, doi:10.1029/2008RG000267.

475 Fujiwara, M., and M. Takahashi (2001), Role of the equatorial Kelvin wave in stratosphere-
476 troposphere exchange in a general circulation model, *J. Geophys. Res.*, **106**, No. D19,
477 22,763-22,780.

478 Fujiwara, M., K. Kita, and T. Ogawa (1998), Stratosphere-troposphere exchange of ozone
479 associated with the equatorial Kelvin wave as observed with ozonesondes and
480 rawinsondes, *J. Geophys. Res.*, **103**, No. D15, 19,173-19,182.

481 Fujiwara, M., K. Kita, S. Kawakami, T. Ogawa, N. Komala, S. Saraspriya, and A. Suropto (1999),
482 Tropospheric ozone enhancements during the Indonesian forest fire events in 1994
483 and in 1997 as revealed by ground-based observations, *Geophys. Res. Lett.*, **26**,
484 2417-2420.

485 Fujiwara, M., F. Hasebe, M. Shiotani, N. Nishi, H. Vömel, and S. J. Oltmans (2001), Water vapor
486 control at the tropopause by equatorial Kelvin waves observed over the Galápagos, *J.*
487 *Geophys. Res.*, **28**, No. 16, 3143-3146.

488 Fujiwara, M., M. K. Yamamoto, H. Hashiguchi, T. Horinouchi, and S. Fukao (2003a) Turbulence
489 at the tropopause due to breaking Kelvin waves observed by the Equatorial
490 Atmosphere Radar, *Geophys. Res. Lett.*, **30** (4), 1171, doi:10.1029/2002GL016278.

491 Fujiwara, M., et al. (2003b), Ozonesonde observations in the Indonesian maritime continent: A
492 case study on ozone rich layer in the equatorial upper troposphere, *Atmos. Env.*, **37**,
493 353-362.

494 Fujiwara, M., et al. (2009), Cirrus observations in the tropical tropopause layer over the
495 western Pacific, *J. Geophys. Res.*, **114**, D09304, doi:10.1029/2008JD011040.

496 Garcia, R. R., and W. J. Randel (2008), Acceleration of the Brewer-Dobson circulation due to
497 increases in greenhouse gases, *J. Atmos. Sci.*, **65**, 2731-2739.

498 Gettelman, A., and P. M. DeF. Forster (2002). A climatology of the tropical tropopause layer, *J.*
499 *Meteor. Soc. Japan*, **80**, No. 4B, 911-924.

500 Gettelman, A., and T. Birner (2007), Insights into tropical tropopause layer processes using
501 global models, *J. Geophys. Res.*, **112**, D23104, doi:10.1029/2001JD001048.

502 Gettelman, A., and M. Hegglin (2009), The Upper Troposphere and Lower Stratosphere,
503 Chapter 7, SPARC CCVal Project, SPARC Tech. Report, in press.

504 Gettelman, A., et al. (2009) The Tropical Tropopause Layer 1960–2100, *Atmos. Chem. Phys.*, **9**,
505 1621-1637.

506 Grant, W. B., R. B. Pierce, S. J. Oltmans, and E. V. Browell (1998) Seasonal evolution of total and
507 gravity wave induced laminae in ozonesonde data in the tropics and subtropics,
508 *Geophys. Res. Lett.* **25**, 1863-1866.

509 Immler, F., K. Krüger, M. Fujiwara, G. Verver, M. Rex, and O. Schrems (2008), Correlation
510 between equatorial Kelvin waves and the occurrence of extremely thin ice clouds at the
511 tropical tropopause, *Atmos. Chem. Physics*, **8**, 4019-4026.

512 Jacob, D. J., et al. (1996), Origin of ozone and NO_x in the tropical troposphere: A photochemical
513 analysis of aircraft observations over the South Atlantic basin, *J. Geophys. Res.*, **101**,
514 24,235– 24,250.

515 Jenkins, G. S., and J.-H. Ryu (2004) Space-borne observations link the tropical Atlantic ozone
516 maximum and paradox to lightning, *Atmos. Chem. Phys.* **4**, 361–375.

517 Jenkins, G. S., J.-H. Ryu, A. M. Thompson, J. C. Witte (2003) Linking horizontal and vertical
518 transport of biomass fire emissions to the tropical Atlantic ozone paradox during the
519 Northern Hemisphere winter season.1999, *J. Geophys. Res.*, 108, 4745, doi: 10.1029/
520 2002JD003297.

521 Johnson, B. J., S. J. Oltmans, H. Vömel, T. Deshler, C. Kroger, and H. G. J. Smit (2002), ECC
522 ozonesondes pump efficiency measurements and sensitivity tests of buffered and
523 unbuffered sensor solutions, *J. Geophys. Res.*, 107(D19), 4393, doi:
524 10.1029/2001JD000557.

525 Kiladis, G. N., M. C. Wheeler, P. T. Haertel, K. H. Straub, P. E. Roundy (2009) Convectively
526 coupled equatorial waves, *Rev. Geophys.*, 47, RG1003, doi:10.1029/2008RG000266.

527 Kley, D., H. G. J. Smit, S. Nawrath, Z. Luo, P. Nedelec, and R. H. Johnson (2007), Tropical Atlantic
528 convection as revealed by ozone and relative humidity measurements, *J. Geophys. Res.*,
529 112, D23109, doi:10.1029/2007JD008599.

530 Konopka, P., J.-U. Grooß, F. Plöger, and R. Müller (2009), Annual cycle of horizontal in-mixing
531 into the lower tropical stratosphere, *J. Geophys. Res.*, **114**, D19111,
532 doi:10.1029/2009JD011955.

533 Krishnamurthi, T. N., M. C. Sinha, M. Kanamitsu, D. Oosterhof, H. Fuelberg, R. Chatfield, D. J.
534 Jacob, and J. Logan (1996), Passive tracer transport relevant to the TRACE A
535 experiment, *J. Geophys. Res.*, 101, 23,889–23,908.

536 Leclair de Bellevue J., A. Réchou, J.L. Baray, G. Ancellet, and R. D. Diab, (2006), Signatures of
537 stratosphere to troposphere, transport near deep convective events in the southern
538 subtropics, *J. Geophys. Res.*, **111**, D24107, doi:10.1029/2005JD006947.

539 Lee, S., D. M. Shelow, A. M. Thompson, and S. K. Miller (2009), QBO and ENSO variability in
540 temperature and ozone from SHADOZ (1998-2005), *J. Geophys. Res.*, doi:10.1029/
541 2009JD013320, submitted.

542 Lehmann, R., and M. Rex (2008), Ascent rates in the tropical lower stratosphere derived from
543 vertical profiles of ozonesonde data. *Geophys. Res. Abstracts*, **10**, EGU2008-A-02555,
544 EGU Spring Assembly.

545 Logan, J. A., and V. W. J. H. Kirchhoff (1986), Seasonal variations of tropospheric ozone at
546 Natal, Brazil, *J. Geophys. Res.*, **91**, 7875– 7888.

547 Logan, J. A., et al. (2003), The quasi-biennial oscillation in equatorial ozone as revealed by
548 ozonesonde and satellite data, *J. Geophys. Res.*, **108**, doi: 10.129/2002JD002170.

549 Logan, J. A., I. A. Megretskaya, R. Nassar, L. T. Murray, L. Zhang, K. W. Bowman, H. M. Worden, M.
550 Luo (2008) Effects of the 2006 El Niño on tropospheric composition as revealed by
551 data from the Tropospheric Emission Spectrometer (TES), *Geophys. Res. Lett.*, **35**,
552 L03816, doi:10.1029/2007GL031698.

553 Loucks, A. L., Evaluation of dynamical sources of ozone laminae in the tropical troposphere and
554 tropical tropopause layer, MS Thesis, Penn State Univ., 2007.

555 Miloshevich, L., H. Vömel, D. N. Whiteman, B. M. Lecht, F. J. Schmidlin, and F. Russo (2006),
556 Absolute accuracy of water vapor measurements from six operational radiosone types
557 launched during AWEX-G and implications for AIRS validation, *J. Geophys. Res.*, **111**,
558 D09S10, doi:10.1029/2005JD006083.

559 Morris, G. A., et al. (2009) Observations of ozone production in a dissipating tropical
560 convective cell during TC4, *J. Geophys. Res.*, submitted. Manuscript available at TC4
561 website. Contact btoon@lasp.colorado.edu for password.

562 Noguchi, K., T. Imamura, K.-I. Oyama, and G. E. Bodeker (2006), A global statistical study on
563 the origin of small-scale ozone vertical structures in the lower stratosphere, *J. Geophys.*
564 *Res.*, **111**, D23105, doi:10.1029/2006JD007232.

565 Oltmans, S. J., et al. (2001) Ozone in the Pacific tropical troposphere from ozonesonde
566 observations, *J. Geophys. Res.*, **106**, 32503-32526.

567 Petropavlovskikh, I., et al. (2009) Low ozone bubbles observed in the tropical tropopause
568 layer during the TC4 campaign in 2007, *J. Geophys. Res.*, submitted. Manuscript
569 available at TC4 website. Contact btoon@lasp.colorado.edu for password.

570 Pickering, K. E., A. M. Thompson, Y. Wang, W.-K. Tao, D. P. McNamara, V. W. J. H. Kirchhoff, B. G.
571 Heikes, G. W. Sachse, J. D. Bradshaw, G. L. Gregory, and D. R. Blake (1996) Convective
572 transport of biomass burning emissions over Brazil during TRACE-A, *J. Geophys. Res.*,
573 **101**, 23,993-24,012.

574 Pierce, R. B., and W. B. Grant (1998), Seasonal evolution of Rossby and gravity wave induced
575 laminae in ozonesonde data obtained from Wallops Island, Virginia, *Geophys. Res. Lett.*,
576 **25**, 1859-1862.

577 Portafaix, T., B. Morel, H. Bencherif, S. Baldy, S. Godin-Beekmann, and A. Hauchecorne (2003),
578 Fine-scale study of a thick stratospheric ozone lamina at the edge of the southern
579 subtropical barrier, *J. Geophys. Res.*, **108** (D6), 4196, doi:10.1029/2002JD002741.

580 Randel, W. J., and F. Wu. (2005), Kelvin wave activity near the equatorial tropopause observed
581 in GPS radio occultation measurements, *J. Geophys. Res.*, **110**, D03102, doi:10.1029/
582 2004JD005006.

583 Randel, W. J., M. Park, F. Wu, and N. Livesey (2007), A large annual cycle in ozone above the
584 tropical tropopause linked to the Brewer-Dobson circulation. *J. Atmos. Sci.*, **64**, 4479-
585 4488.

586 Randel, W. J., R. R. Garcia, N. Calvo, and D. Marsh (2009), ENSO influence on zonal mean
587 temperature and ozone in the tropical lower stratosphere, *Geophys. Res. Lett.*, **36**,
588 L15822, doi: 10.1029/2009GL039343.

589 Randriambelo, T., J-L. Baray, S. Baldy, A. M. Thompson, S. J. Oltmans, and P. Keckhut (2003),
590 Investigation of the short-term variability of tropical tropospheric ozone, *Annales*
591 *Geophysicaes*, **21**, 2095-2106.

592 Roundy, P. E., and W. M. Frank (2004a), A climatology of waves in the equatorial Region. *J.*
593 *Atmos. Sci.*, **61**, 2105-2132.

594 Roundy, P. E., and W. M. Frank (2004b), Effects of low-frequency wave interactions on
595 intraseasonal oscillations. *J. Atmos. Sci.*, **61**, 3025-3040.

596 Ryu, J-H., S. Lee and S.-W. Son, Vertically propagating Kelvin waves and tropical tropopause
597 variability, *J. Atmos. Sci.*, **65**, 1817-1867.

598 Ryu, J-H., and S. Lee (2009) Effect of Tropical waves on the tropical tropopause-transition-
599 layer upwelling. *J. Atmos. Sci.*, to be submitted.

600 Selkirk, H. B., H. Vömel, J. M. Valverde Canossa, L. Pfister, J. A. Diaz, W. Fernández, J. Amador, W.
601 Stolz, and G. Peng, The detailed structure of the tropical upper troposphere and lower
602 stratosphere as revealed by balloonsonde observations of water vapor, ozone,
603 temperature and winds during the NASA TCSP and TC4 Campaigns, *J. Geophys. Res.*,
604 submitted. ** Manuscript available at TC4 website. Contact btoon@lasp.colorado.edu
605 for password.

606 Shiotani, M. (1992), Annual, quasi-biennial and El Nino-Southern Oscillation (ENSO). time-
607 scale variations in Equatorial total ozone, *J. Geophys. Res.*, **97**, 7625-7634.

608 Smit, H. G. J., et al. (2007), Assessment of the performance of ECC-ozonesondes under quasi-
609 flight conditions in the environmental simulation chamber: Insights from the Jülich
610 Ozone Sonde Intercomparison Experiment (JOSIE), *J. Geophys. Res.*, **112**, D19306, doi:
611 10.1029/ 2006JD007308.

612 Smit, H. G. J., and ASOPOS-panel (2009), Quality assurance and quality control for ozonesonde
613 measurements in GAW, WMO Global Atmospheric Watch report series, in press.

614 Smith, C.A. and P. Sardeshmukh (2000) , The effect of ENSO on the intraseasonal variance of
615 surface temperature in winter., *Intl J. Climatol.*, **20**, 1543-1557.

616 Son, S. W., and S. Lee (2007), Intraseasonal variability of the zonal mean tropical tropopause
617 height. *J. Atmos. Sci.*, **64**, 2695-2706.

618 Smyth, S. B., et al. (1996) Factors influencing the upper free tropospheric distribution of
619 reactive nitrogen over the South Atlantic during the TRACE-A experiment, *J. Geophys.*
620 *Res.*, **101**, 24165-24186.

621 Suzuki, J., and M. Shiotani (2008), Space-time variability of equatorial Kelvin waves and
622 intraseasonal oscillations around the tropical tropopause, *J. Geophys. Res.*, **113**,
623 D16110, doi:10.1029/2007JD009456.

624 Takashima, H., M. Shiotani, M. Fujiwara, N. Nishi, and F. Hasebe (2008), Ozonesonde
625 observations at Christmas Island (2°N, 157°W) in the equatorial central Pacific, *J.*
626 *Geophys. Res.*, **113**, D10112, doi:10.1029/2007JD009374.

627 Takashima, H., and M. Shiotani, (2007), Ozone variation in the tropical tropopause layer as
628 seen from ozonesonde data, *J. Geophys. Res.*, **112**, D11123, doi:10.1029/2006JD008322.

629 Teitelbaum, H., Ovarlez, J., Kelder, H., & Lott, F. (1994), Some observations of gravity-wave-
630 induced structure in ozone and water vapour during EASOE, *Geophys. Res. Lett.*, **21**,
631 1483-1486.

632 Teitelbaum, H., M. Moustouai, J. Ovarlez, and H. Kelder (1996), The role of atmospheric waves
633 in the laminated structure of ozone profiles at high latitudes, *Tellus*, **48A**, 442-455.

634 Thompson, A.M., "Intercontinental Transport of Ozone from Tropical Biomass Burning" in A.
635 Stohl, ed. *Intercontinental Transport*, Springer-Verlag, Chapter 9, 2004.

636 Thompson, A. M., and R. D. Hudson (1999), Tropical Tropospheric Ozone (TTO) maps from
637 Nimbus-7 and Earth-Probe TOMS by the modified-residual method: Evaluation with
638 sondes, ENSO signals and trends from Atlantic regional time series, *J. Geophys. Res.*,
639 **104**, 26,961-26,975.

640 Thompson, A. M., et al. (1996) Where did tropospheric ozone over southern Africa and the
641 tropical Atlantic come from in October 1992? Insights from TOMS, GTE/TRACE-A and
642 SAFARI-92, *J. Geophys. Res.*, **101**, 24,251-24,278.

643 Thompson, A. M., W.-K. Tao, K. E. Pickering, J. R. Scala, and J. Simpson (1997) Tropical deep
644 convection and ozone formation, *Bull. Amer. Met. Soc.*, **78**, 1,043-1,054.

645 Thompson, A. M., B. G. Doddridge, J. C. Witte, R. D. Hudson, W. T. Luke, J. E. Johnson, B. J.
646 Johnson, S. J. Oltmans and Weller (2000), A tropical Atlantic ozone paradox: Shipboard
647 and satellite views of a tropospheric ozone maximum and wave-one in January-
648 February 1999, *Geophys. Res. Lett.*, **27**, 3317-3320.

649 Thompson, A. M., J. C. Witte, R. D. Hudson, H. Guo, J. R. Herman, M. Fujiwara (2001), Tropical
650 tropospheric ozone and biomass burning, *Science*, **291**, 2128-2132.

651 Thompson, A. M., J. C. Witte, M. T. Freiman, N. A. Phahlane, G. J. R. Coetzee, Lusaka, Zambia,
652 during SAFARI-2000: Convergence of local and imported ozone pollution (2002),
653 *Geophys. Res. Lett.*, **29**, 1976, doi: 10.1029/2002GL015399.

654 Thompson, A. M., et al. (2003a), Southern Hemisphere Additional Ozonesondes (SHADOZ)
655 1998-2000 tropical ozone climatology. 1. Comparison with TOMS and ground-based
656 measurements, *J. Geophys. Res.*, **108**, 8238, doi: 10.1029/2001JD000967.

657 Thompson, A. M., et al. (2003b), Southern Hemisphere Additional Ozonesondes (SHADOZ)
658 1998-2000 tropical ozone climatology. 2. Tropospheric variability and the zonal
659 wave-one, *J. Geophys. Res.*, **108**, 8241, doi: 10.1029/2002JD002241.

660 Thompson, A. M., et al. (2007a), IONS (INTEX Ozonesonde Network Study, 2004). 1.
661 Summertime UT/LS (Upper Troposphere/Lower Stratosphere) ozone over
662 northeastern North America, *J. Geophys. Res.*, **112**, D12S12, doi:
663 10.1029/2006JD007441.

664 Thompson, A. M., et al. (2007b), IONS (INTEX Ozonesonde Network Study, 2004): 2.
665 Tropospheric ozone budgets and variability over northeastern North America, *J.*
666 *Geophys. Res.*, **112**, D12S13, doi: 10.1029/2006JD007670.

667 Thompson, A. M., J. C. Witte, H. G. J. Smit, S. J. Oltmans, B. J. Johnson, V. W. J. H. Kirchhoff, F. J.
668 Schmidlin (2007c), Southern Hemisphere Additional Ozonesondes (SHADOZ) 1998-
669 2004 tropical ozone climatology. 3. Instrumentation, station variability, evaluation
670 with simulated flight profiles, *J. Geophys. Res.*, **112**, D03304, doi: 10.1029/
671 2005JD007042.

672 Thompson, A. M., et al. (2009), Convective and wave signatures in ozone profiles over the
673 equatorial Americas: Views from TC4 (2007) and SHADOZ, *J. Geophys. Res.*, doi:
674 10.1029/2009JD012909, submitted. ** Manuscript available at TC4 website. Contact
675 btoon@lasp.colorado.edu for password.

676 Thouret, V., et al. (2009), An overview of two years of ozone soundings over Cotonou as part
677 of AMMA, *Atmos. Chem. Phys.*, **9**, 6157-6174.

678 Toon, O. B., et al. (2009), Planning and implementation of the Tropical Composition, Cloud and
679 Climate Coupling Experiment (TC4), *J. Geophys. Res.*, submitted. ** Manuscript
680 available at TC4 website. Contact btoon@lasp.colorado.edu for password.

681 Tsuda, T., Y. Murayama, H. Wiryosumarto, S. W. B. Harijino, and S. Kato (1994), Radiosonde
682 observations of equatorial atmospheric dynamics over Indonesia. 1. Equatorial waves
683 and diurnal tides. *J. Geophys. Res.*, **99**, 10491-10505.

684 Vömel, H., et al., (2002), Balloon-borne observations of water vapor and ozone in the tropical
685 upper troposphere and lower stratosphere, *J. Geophys. Res.*, **107** (D14), 4210,
686 doi:10.1029/2001JD000707.

687 Vömel, H., H. Selkirk, L. Miloshevich, J. Valverde, J. Valdés, E. Kyrö, R.Kivi, W. Stolz, G. Peng, and
688 J. A. Diaz (2007), Radiation dry bias of the Vaisala RS92 humidity sensor, *J. Atmos.*
689 *Oceanic Technol.*, **24**, 953–963.

690 Wheeler, M., and G.N. Kiladis (1999), Convectively Coupled equatorial waves: Analysis of
691 clouds and temperature in the wavenumber–frequency domain, *J. Atmos. Sci.*, **56**,
692 374–399

693 Witte, J. C., M. R. Schoeberl, A. R. Douglass, and A. M. Thompson (2008), The Quasi-biennial
694 Oscillation in tropical ozone from SHADOZ and HALOE, *Atmos. Chem. Phys.*, **8**,
695 3929-3936.

696 Yonemura, S., H. Tsuruta, S. Kawashima, and S. Sudo (2002), Tropospheric ozone climatology
697 over Peninsular Malaysia from 1992 to 1999, *J. Geophys. Res.*, **107**(D15) 4229,
698 10.1029/2001JD000993.

699 Yang Q., Q. Fu, J. Austin, A. Gettelman, F. Li, H. Vömel (2008), Observationally derived and
700 general circulation model simulated tropical stratospheric upward mass fluxes, *J.*
701 *Geophys. Res.*, **113**, D00B07, doi:10.1029/2008JD009945.

702 Zhou X. L. and J. R. Holton (2002), Intraseasonal variations of tropical cold-point tropopause
703 temperature. *J. Atmos. Sci.*, **15**, 1460-1473.

TABLE 1 - SHADOZ station locations used here, with years of record and sonde numbers.

SITE	Latitude, Longitude	Years of Data Record	SN
Irene	25S, 28E	1999-2007	231
Nairobi	1S, 35E	1999-2007	422
Malindi	1S, 37E	1999-2005	102
La Réunion	21S, 55E	1998-2007	277
Kuala Lumpur	2.7N, 102E	1998-2007	236
Watakosek	7.5S, 114E	1998-2007	262
Fiji	18S, 178E	1998-2007	254
Am. Samoa	14S, 171W	1998-2007	363
Paramaribo	5N, 55W	1999-2007	345
San Cristóbal	1S, 90W	1999-2007	345
Natal (Brazil)	6S, 35W	1998-2007	346
Ascension Island	8S, 15W	1998-2007	460

Table 2. Summary of column ozone amount (DU), Mean Gravity Wave Index (GWI), Rossby Wave Index (RWI) and correlations of GWI and RWI with ENSO and QBO indices. **Red values** denote statistical significance (95% or more).

Site	Mean O ₃ (20km, DU)	Mean GWI (%)	Mean RWI (%)	GWI Corr w/ ENSO Index	RWI Corr w/ ENSO Index	GWI Corr w/ QBO	RWI Corr w/ QBO
Nairobi	55.2	16.6	6.68	0.00	0.08	0.19	0.14
Natal	43.8	10.9	3.76	-0.07	-0.09	0.19	0.20
Watak.	37.4	18.5	10.5	-0.14	0.14	-0.07	-0.01
K. Lumpur	29.5	19.4	3.00	-0.25	0.26	-0.11	-0.13
Am.Samoa	37.2	16.1	8.71	0.23	0.07	0.11	-0.12
Irene	52.6	5.14	2.82	-0.06	0.08	0.11	-0.06
Fiji	57.4	12.6	8.40	-0.12	0.13	0.07	-0.13
San Cris.	38.5	12.6	5.25	0.05	0.27	0.14	0.14
Paramar.	41.6	7.85	6.30	0.04	0.21	0.22	-0.01
Ascension	53.6	8.35	2.34	-0.22	0.10	0.06	-0.02
Reunion	53.4	5.83	4.86	-0.05	-0.16	-0.19	-0.04

FIGURE CAPTIONS

Figure 1

(a) Profile of ozone partial pressure (black) with temperature (red) and relative humidity measured by ozonesonde-radiosonde combination, measured at Suva, Fiji, SHADOZ site, taken from SHADOZ website: <<http://croc.gsfc.nasa.gov/shadoz>>; (b) Normalized O_3 (solid line), potential temperature (θ , dotted line), with correlation between the two quantities (dashed), as determined in laminar identification (LID). Correlation criteria for Rossby wave (RW) are within vertical lines between -0.3 and +0.3 (light blue). By requiring an O_3 layer amplitude of 0.1 (10%), the region designated RW is restricted to darker blue. Gravity wave (GW) criterion by LID method (*Pierce and Grant* [1998; see their Figure 1] and *Thompson et al. 2007a*; Figure 3]) calls for normalized O_3 and θ correlation to reach 0.7 (vertical line). GW layers are light green, but only dark green is counted in the GWI (Gravity Wave Index), given a 10% layer-amplitude requirement for O_3 . BL (boundary-layer), FT (free-troposphere), TTL (tropopause transition layer), LS (lower stratosphere) segments.

Figure 2

Ozone mixing ratio curtains, surface to 18.5 km, over 10-yr SHADOZ record at representative sites: Africa-western Indian Ocean, (a) Nairobi and (b) La Réunion; eastern Indian Ocean, [c] Watukosek, Java, (d) Kuala Lumpur; Pacific, (e) Samoa and (f) San Cristóbal; South American and Atlantic (g) Natal and (h) Ascension. San Cristóbal soundings began in 1999. Frequency is nominally weekly but gaps sometimes occur (cf Figure 9, *Thompson et al., 2003b*).

Figure 3

Mean monthly mixing ratio in the troposphere, TTL and LS, 0-20 km based on 1998-2007 soundings for: (a) Nairobi; (b) Watukosek; [c] Kuala Lumpur; (d) Fiji; (e) San Cristóbal; (f)

Natal.

Figure 4

Monthly averaged laminae *amplitude* for SHADOZ sites: (a) Nairobi; (b) Watukosek; (c) Kuala Lumpur; (d) Samoa; (e) Natal. Number of sondes used is at bottom of panel.

Figure 5 Monthly averaged laminae GW frequency at: (a) Nairobi; (b) Watukosek; (c) Kuala Lumpur; (d) Samoa; (e) Natal. Number of sondes at bottom of panel.

Figure 6 Same as Figure 5 for RW frequency.

Figure 7 Annually averaged GW frequency (a) and RW frequency (b) as function of altitude for twelve SHADOZ stations.

Figure 8

Contours of (a) GW frequency, averaged between 15-20 km, as function of month and site. (b) same as (a) but for RW average below 12 km.

Figure 9

Time-series of GW and RW indices (GWI and RWI) from 1998 through 2007: (a) Nairobi; (b) Watukosek; (c) Kuala Lumpur; (d) Samoa; (e) Natal.

SUPPLEMENTARY Figures

Figure S-1 Curtains of RH from radiosondes at representative SHADOZ to 12 km. Tendencies of humidity sensors vary considerably in the upper troposphere; some are known to have a dry bias (*Miloshevich et al., 2006; Vömel et al., 2002; 2007; R. Stuebi, personal communication, 2009*). Thus, absolute differences among sites shown are not meaningful, although temporal variations within a single data set may be useful.

Figure S-2 Same as Figure 2, except for TTL-LS ozone curtains, 15-20 km.

Figure S-3 GWI and RWI time-series from 1998 through 2007 for: (a) Fiji; (b) Ascension; (c) Irene; La Réunion.

Figure 1

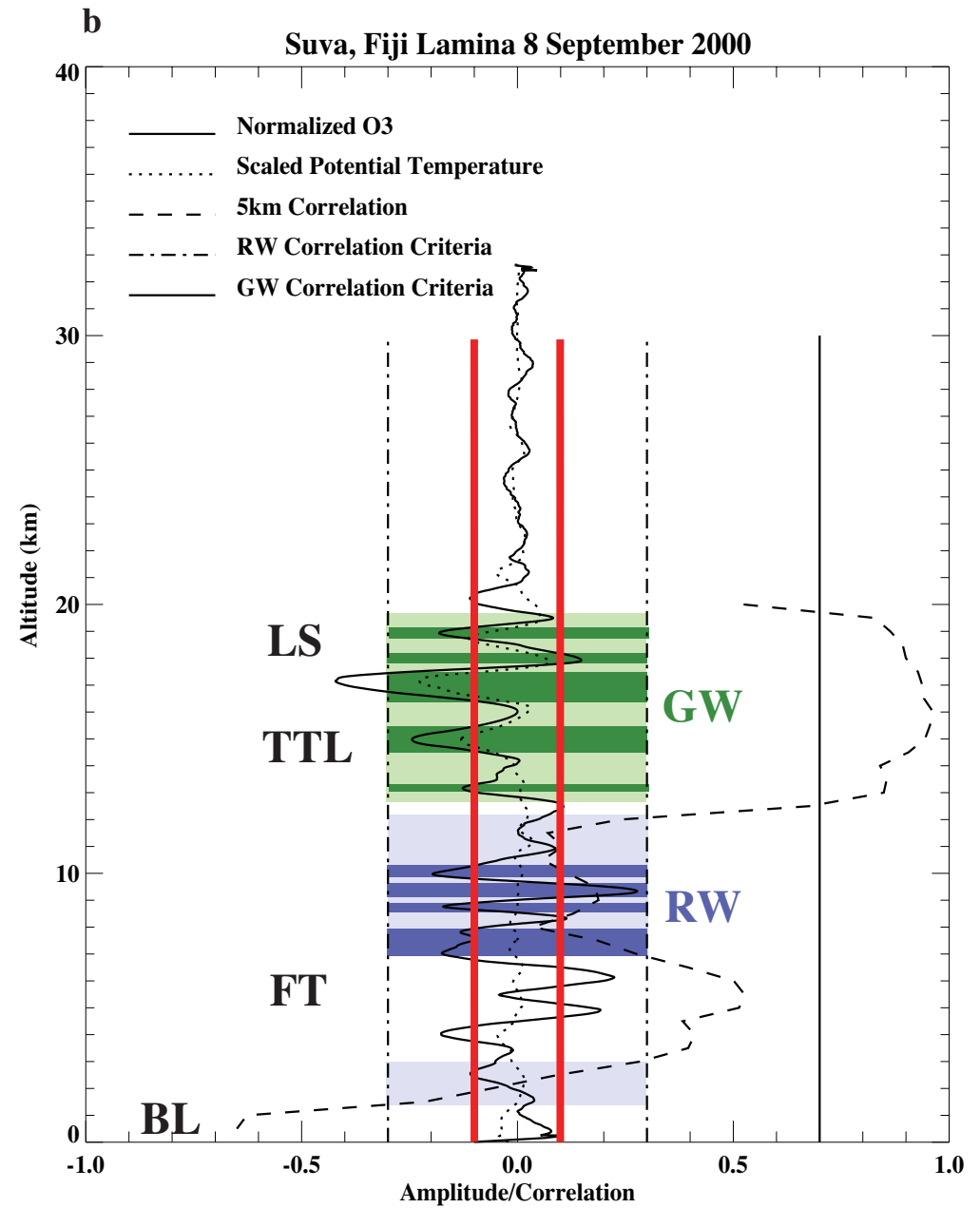
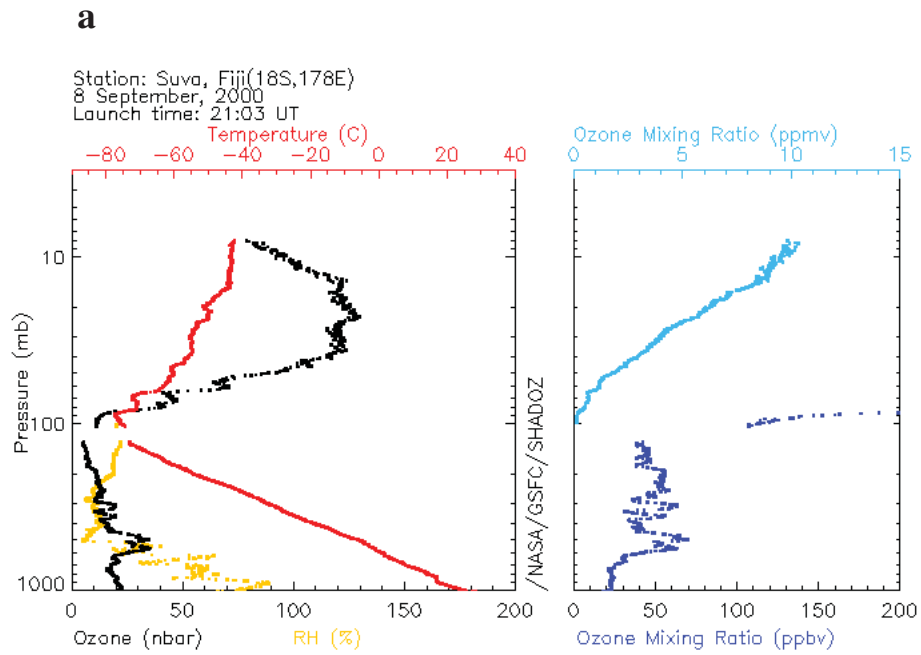


Figure 2

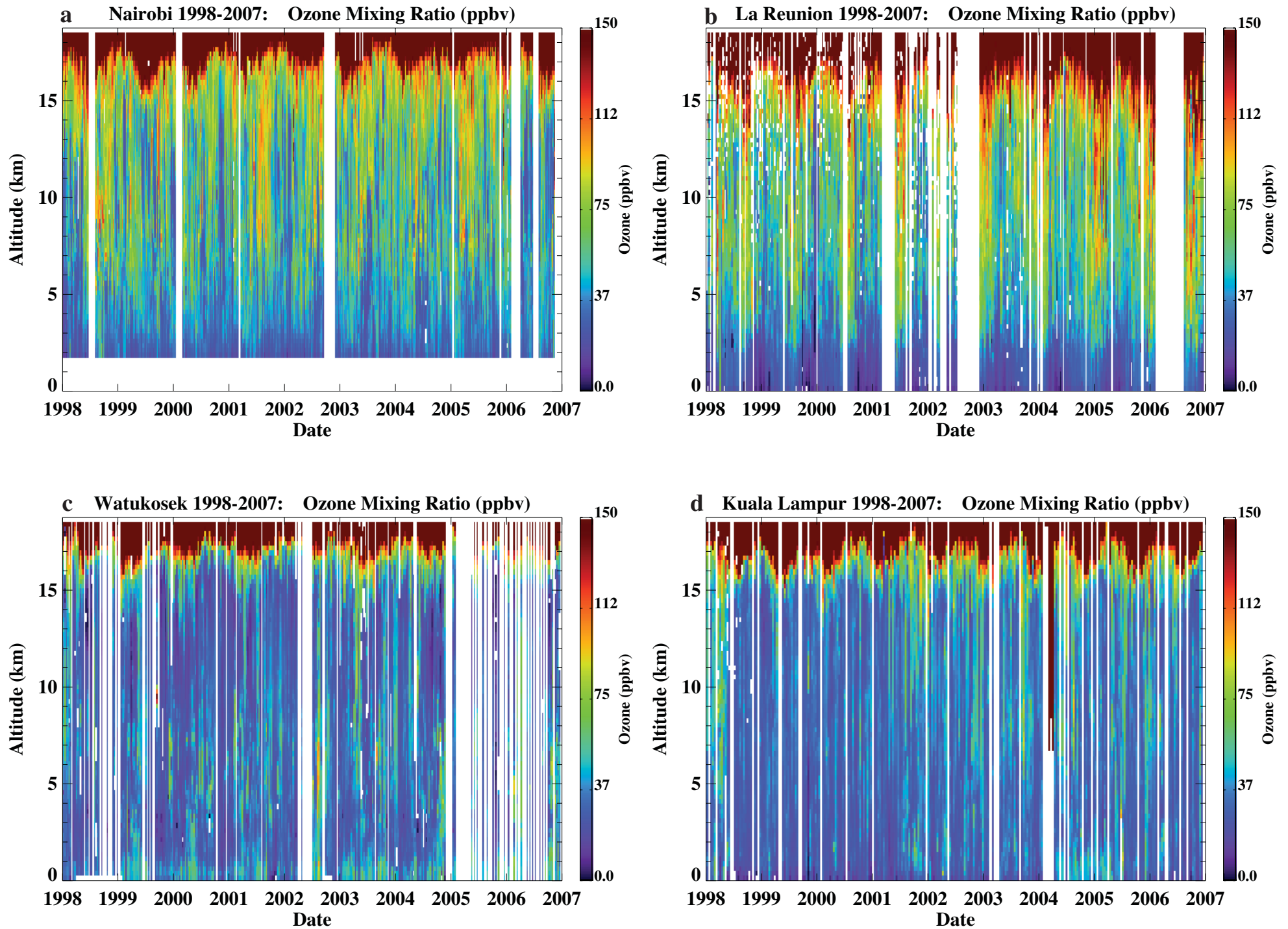


Figure 2 (continued)

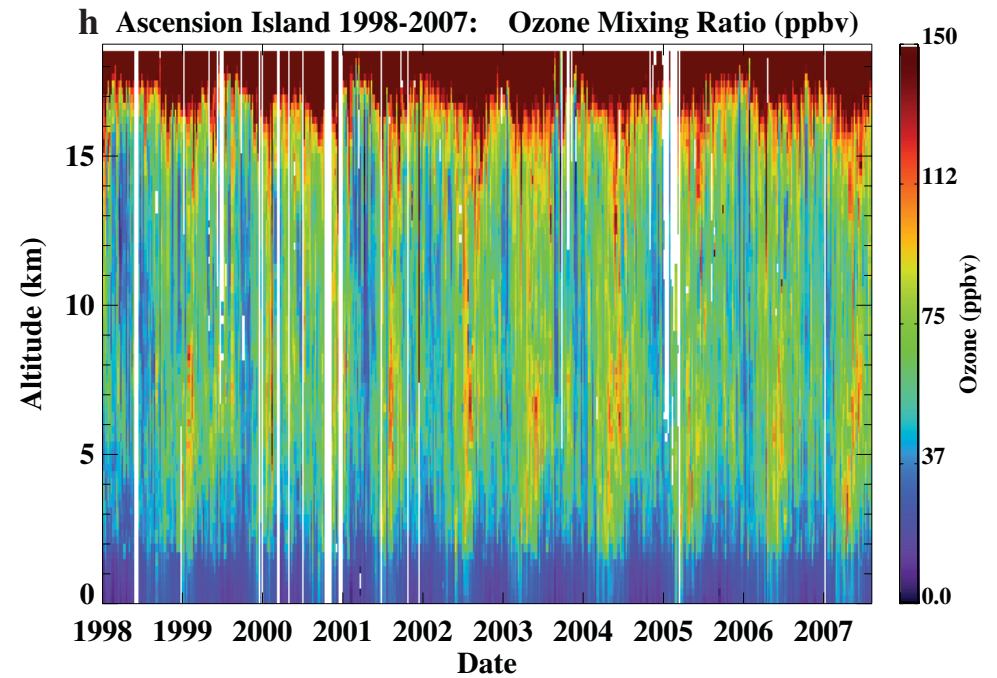
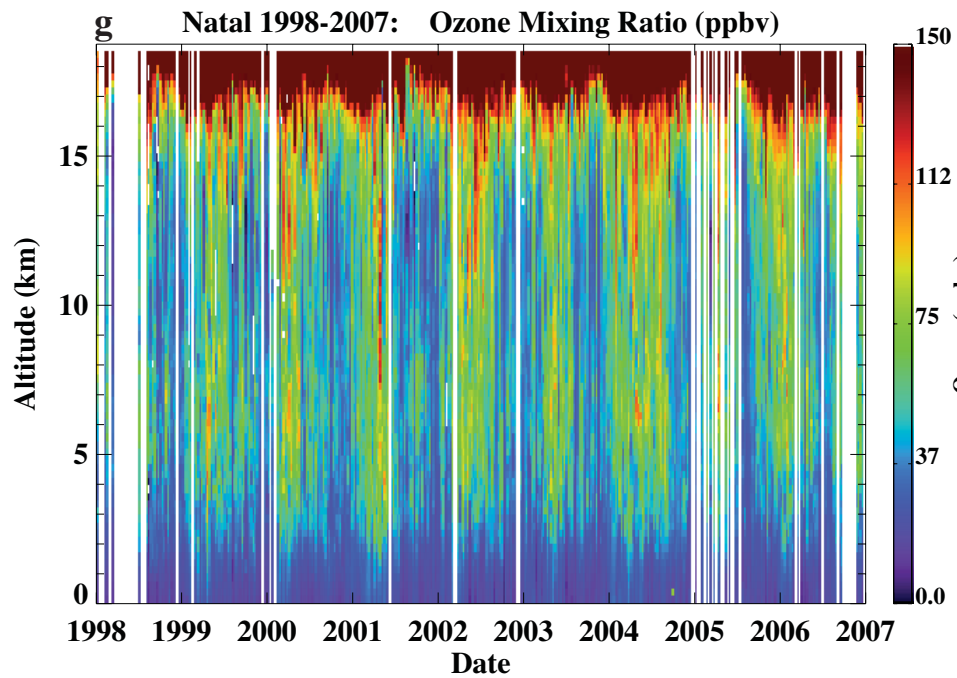
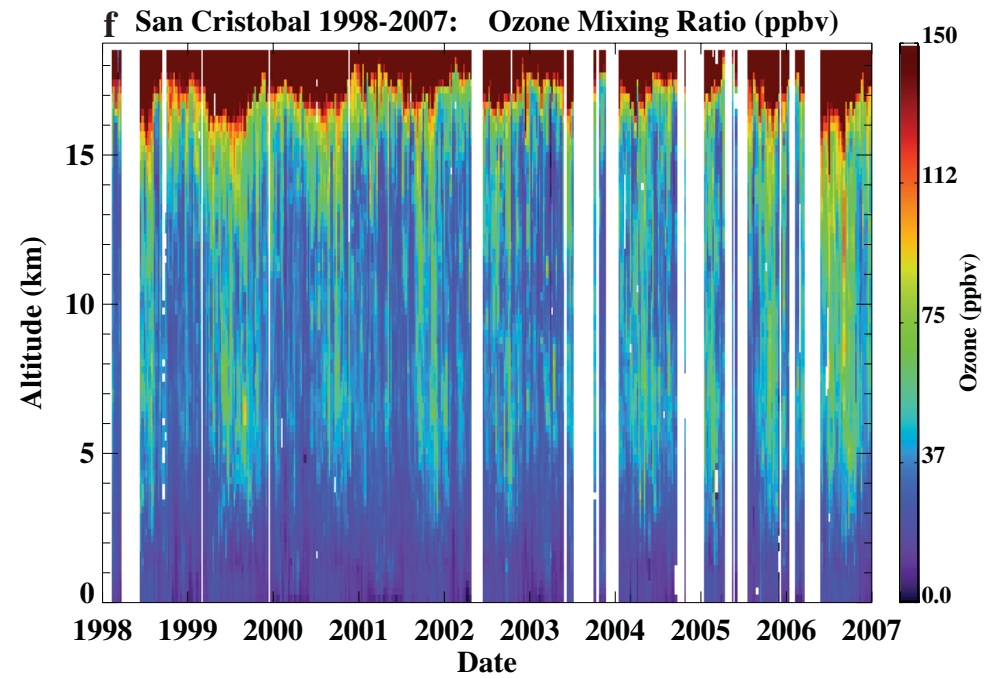
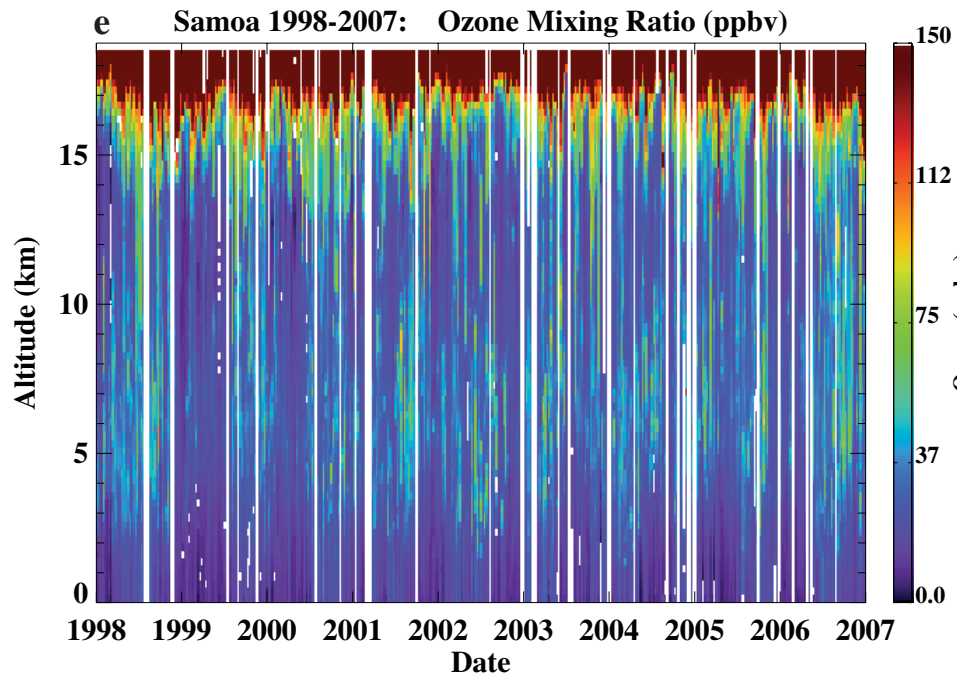


Figure 3

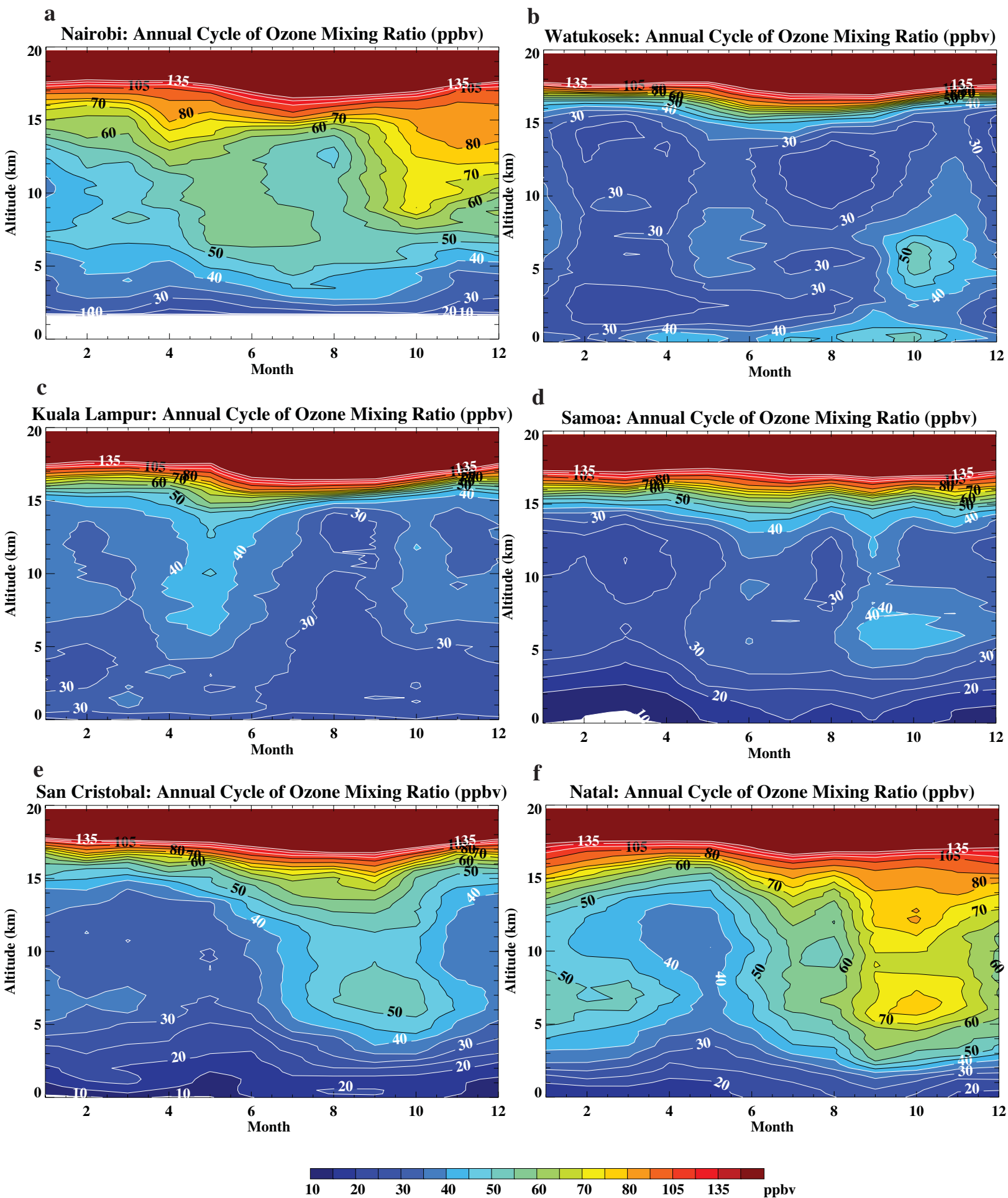
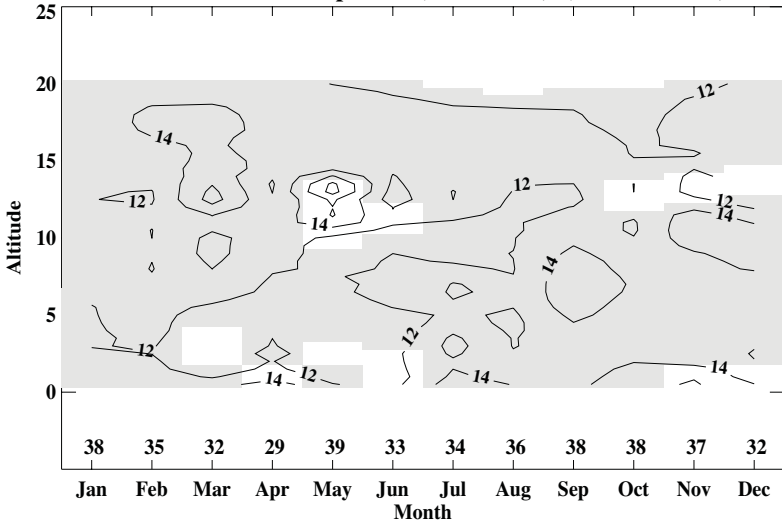
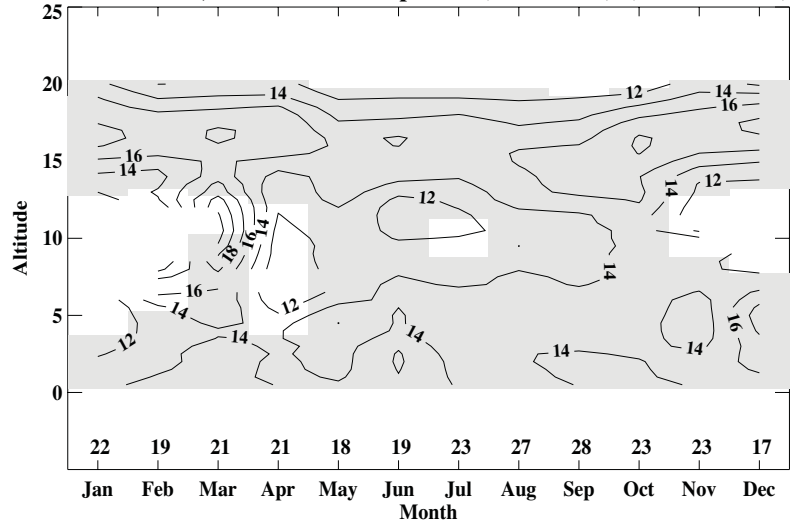


Figure 4

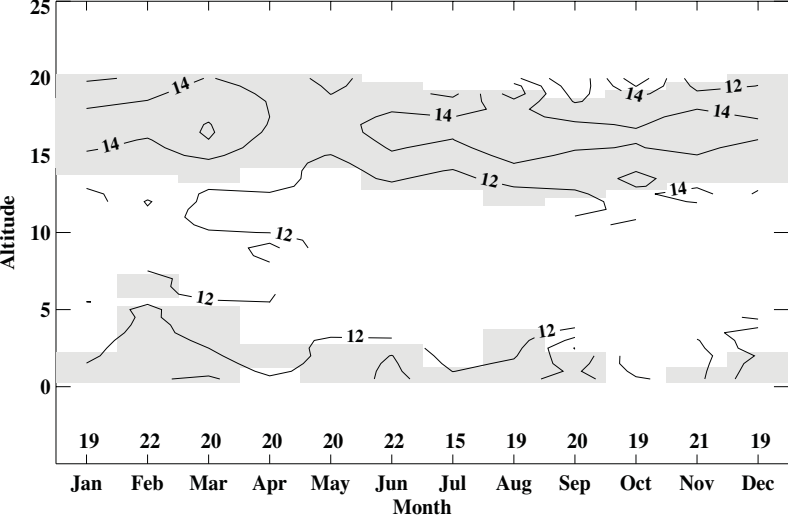
a Nairobi Lamina Amplitude (% of mean) (Total Lamina)



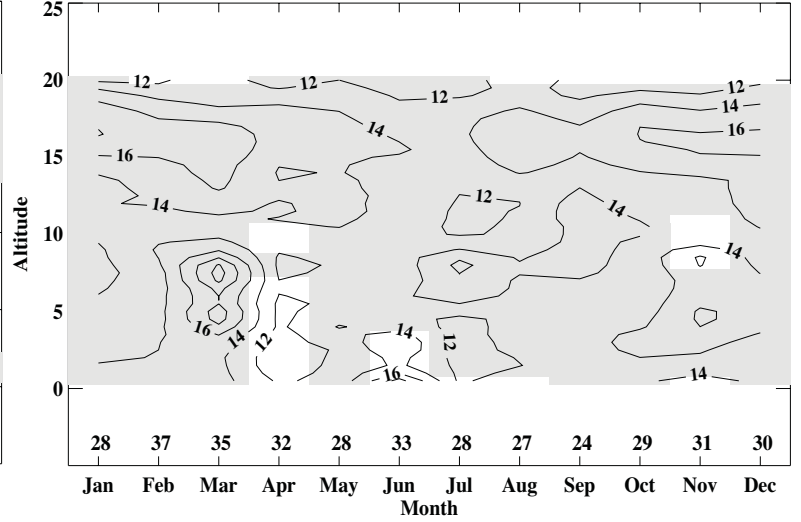
b Watukoskek, Java Lamina Amplitude (% of mean) (Total Lamina)



c Kuala Lumpur Lamina Amplitude (% of mean) (Total Lamina)



d American Samoa Lamina Amplitude (% of mean) (Total Lamina)



e Natal, Brazil Lamina Amplitude (% of mean) (Total Lamina)

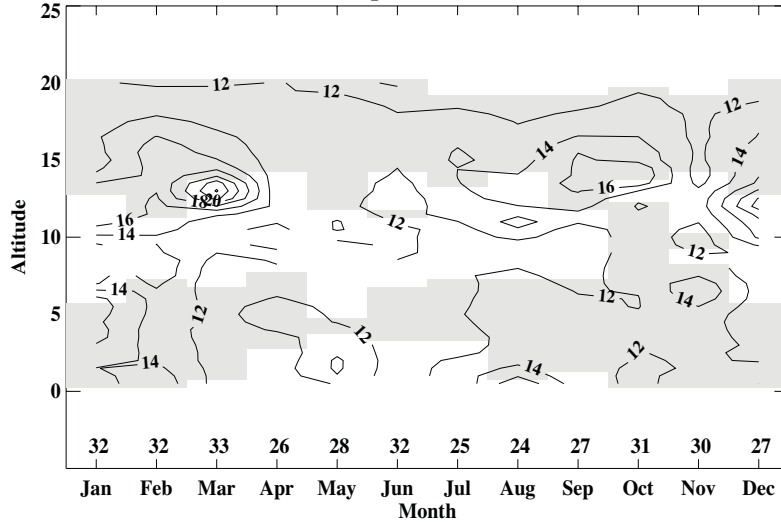


Figure 5

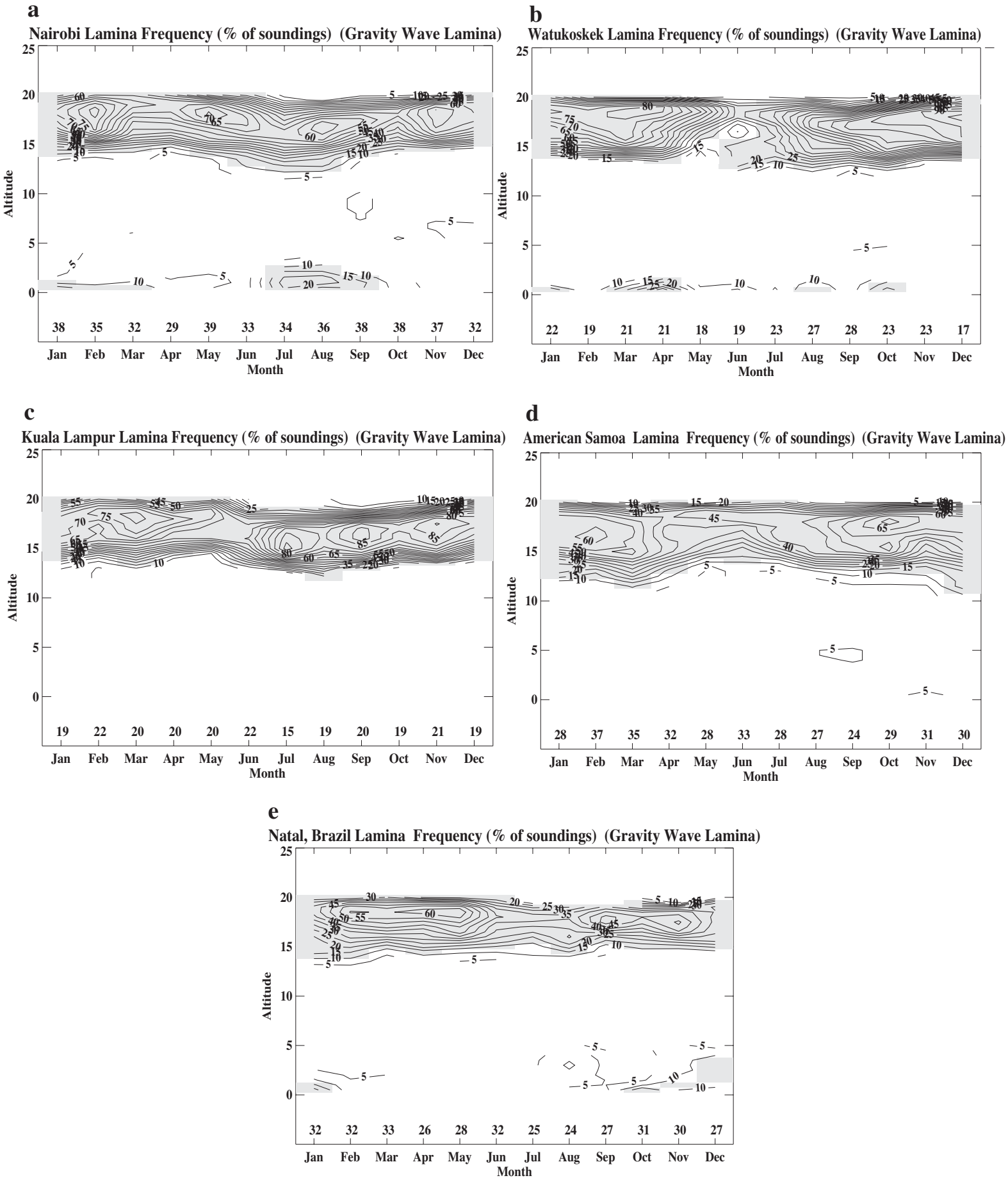


Figure 6

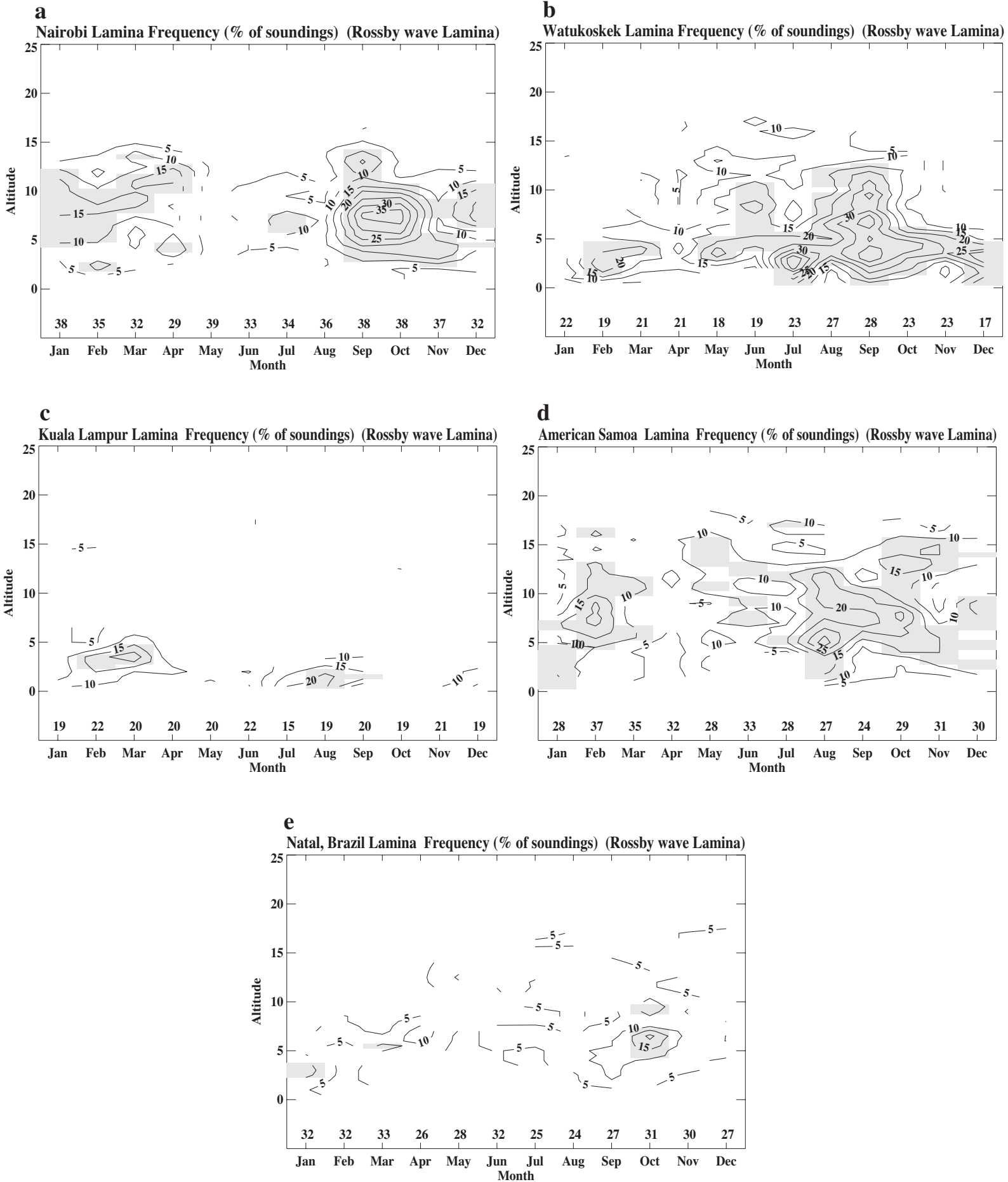


Figure 7

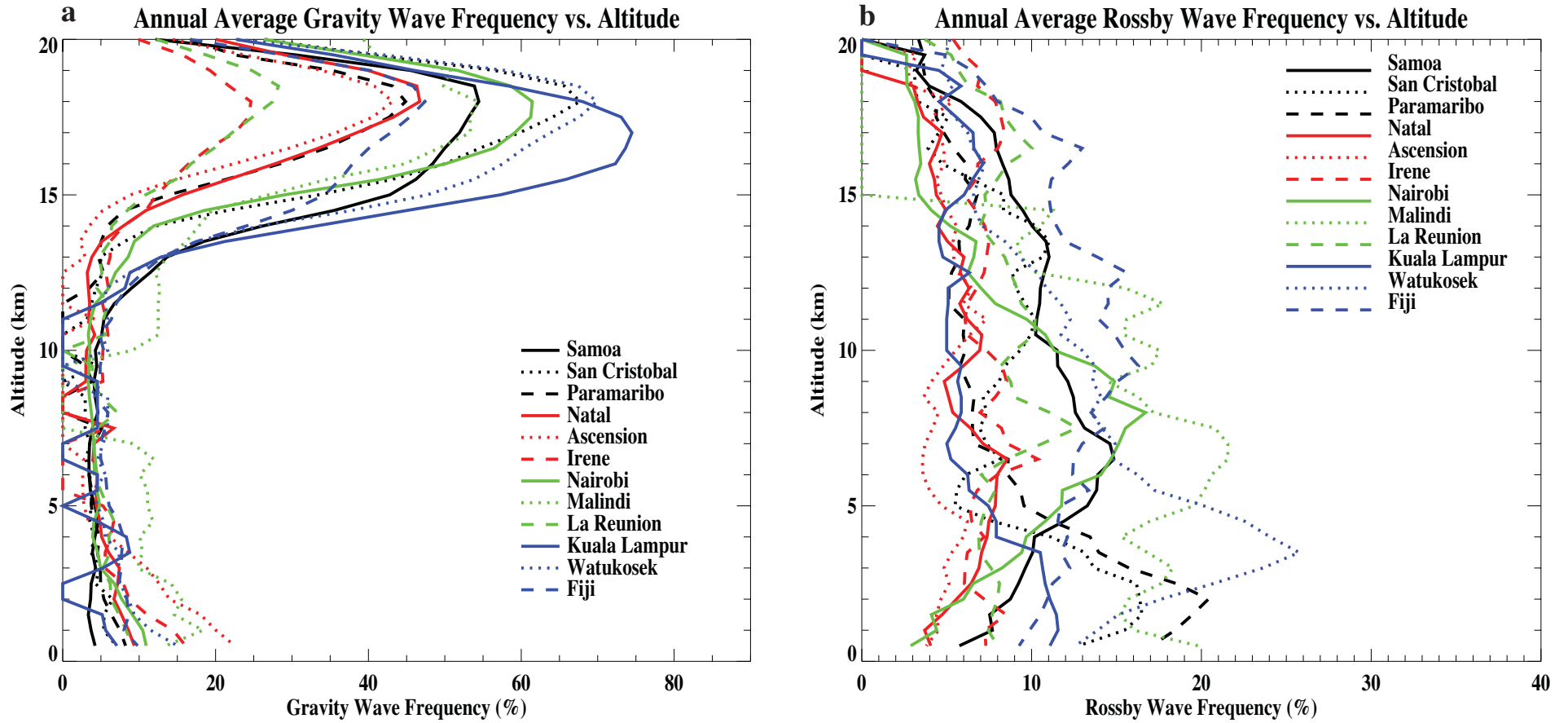


Figure 8

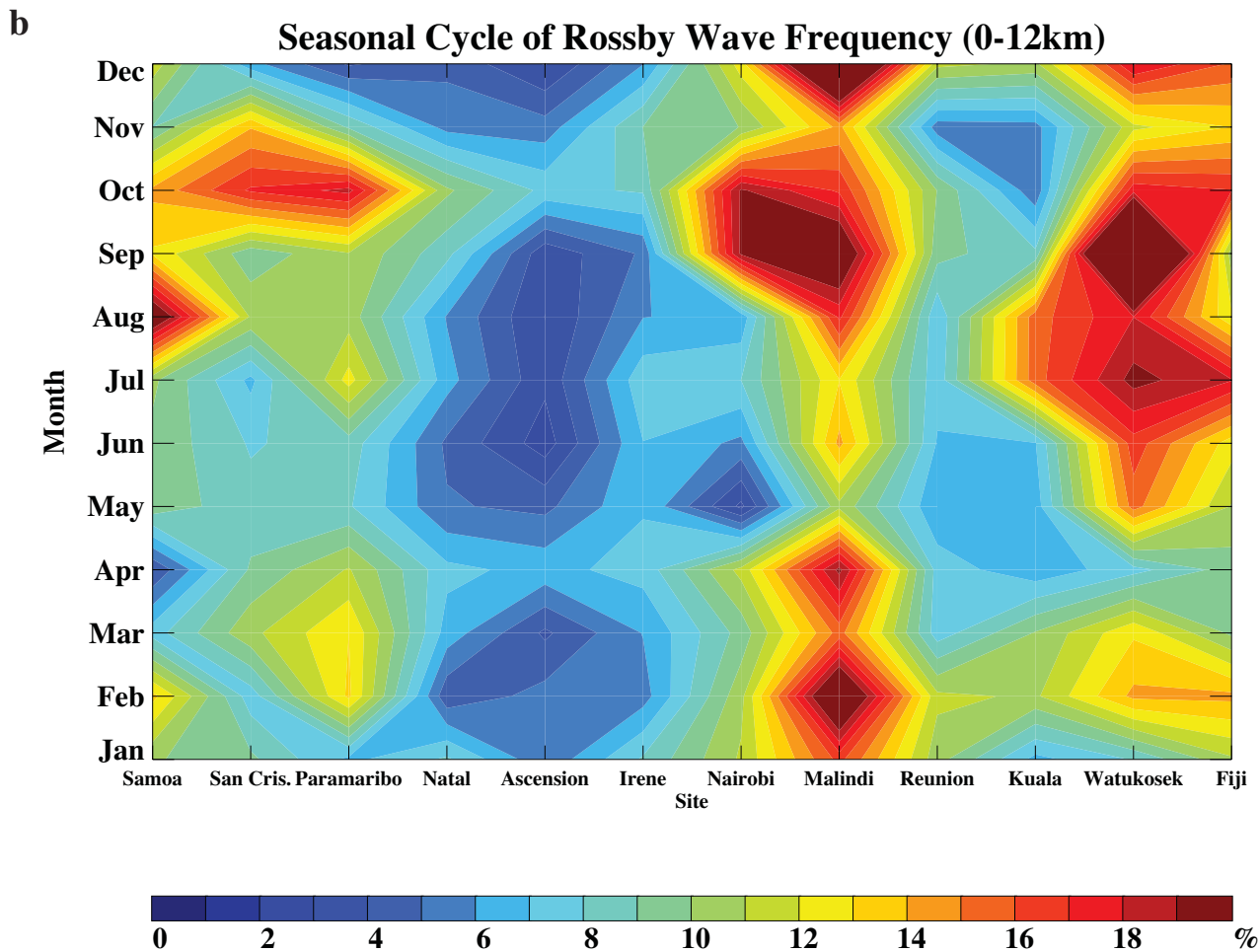
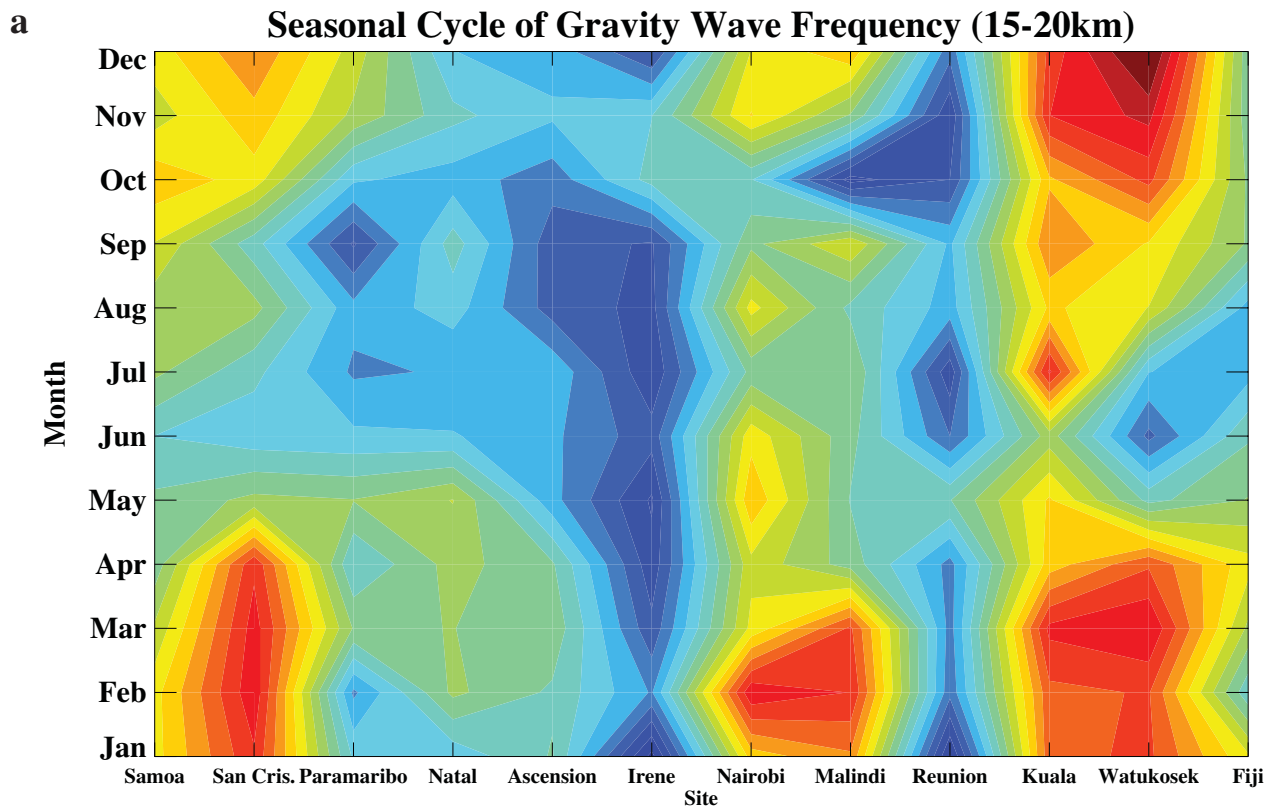


Figure 9

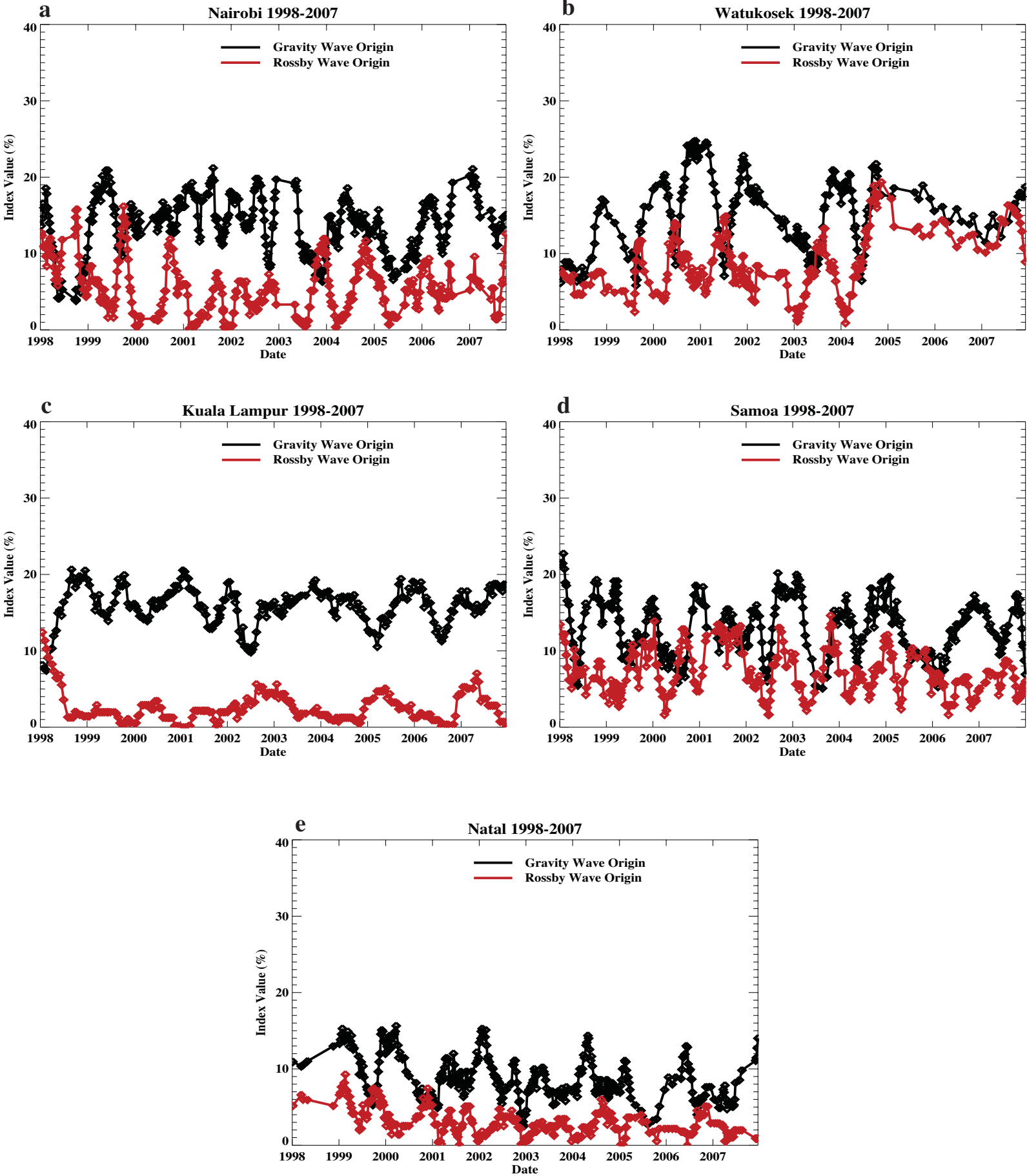


Figure S1

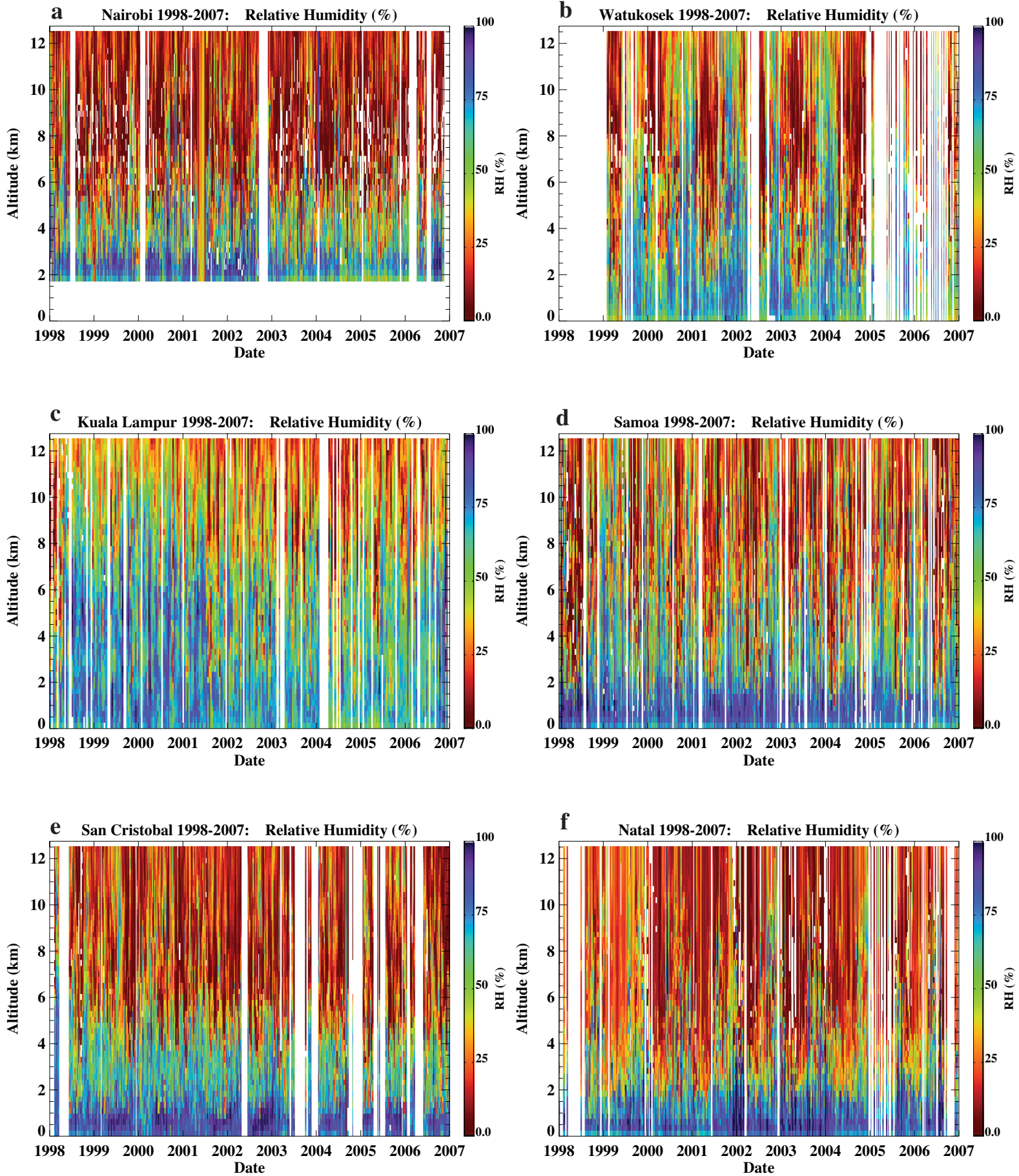


Figure S2

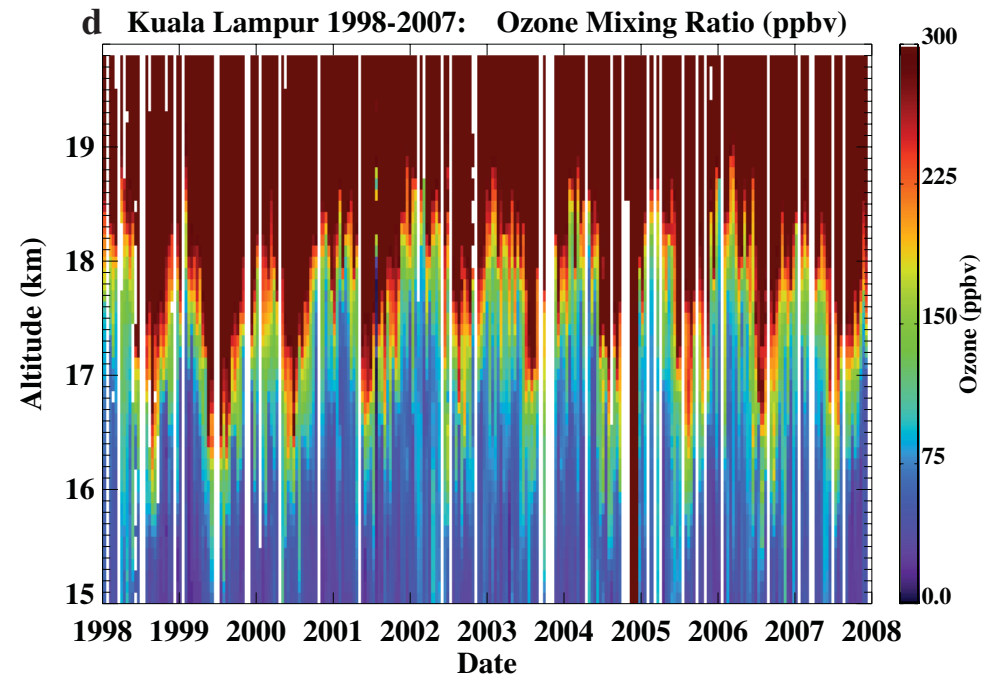
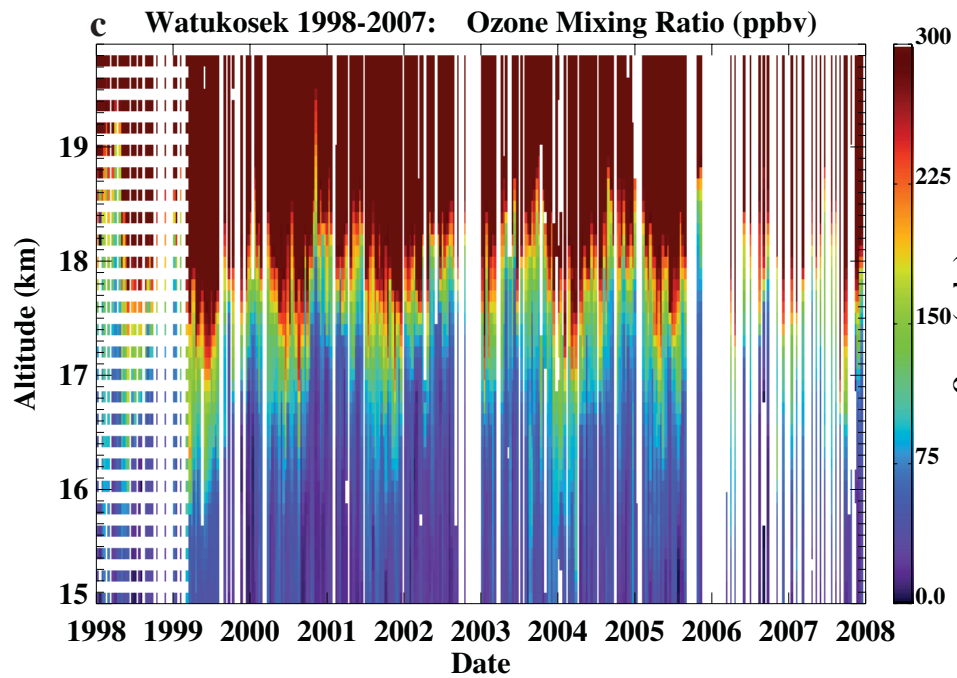
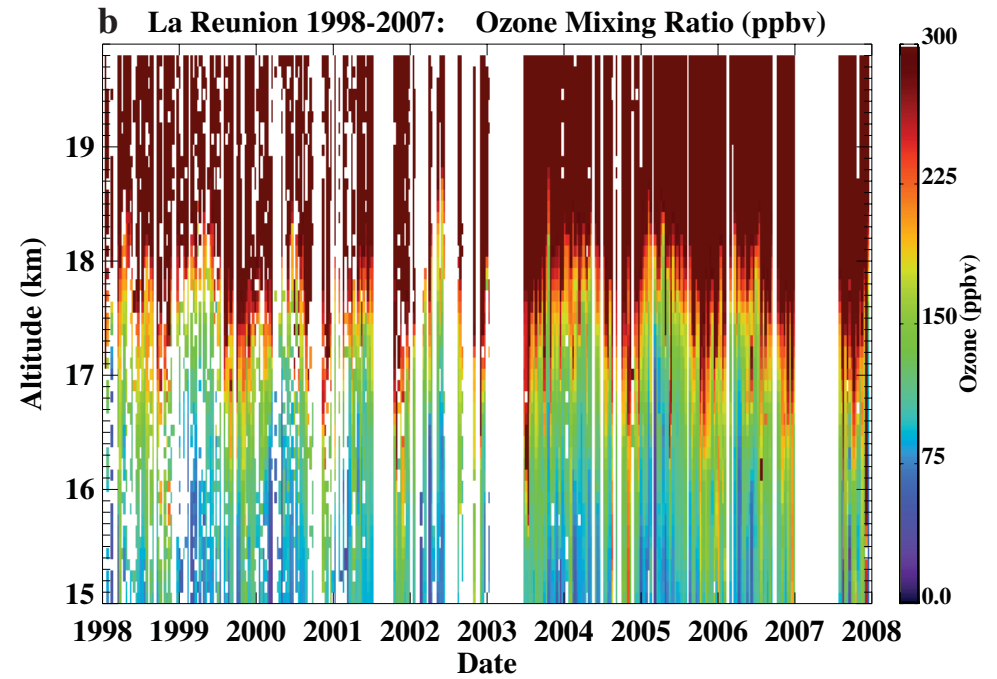
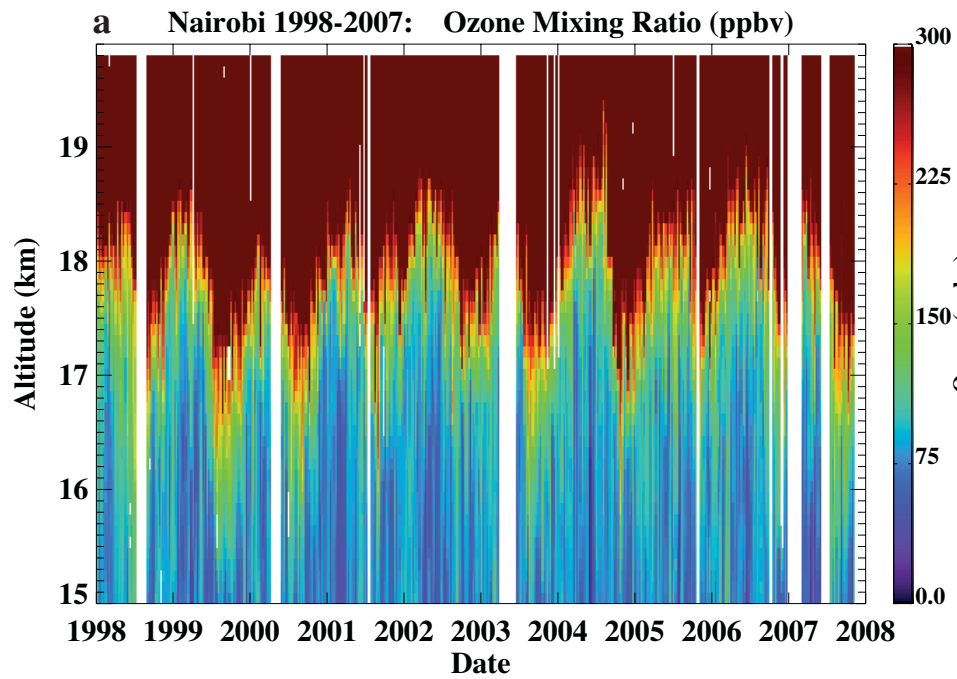


Figure S2 (continued)

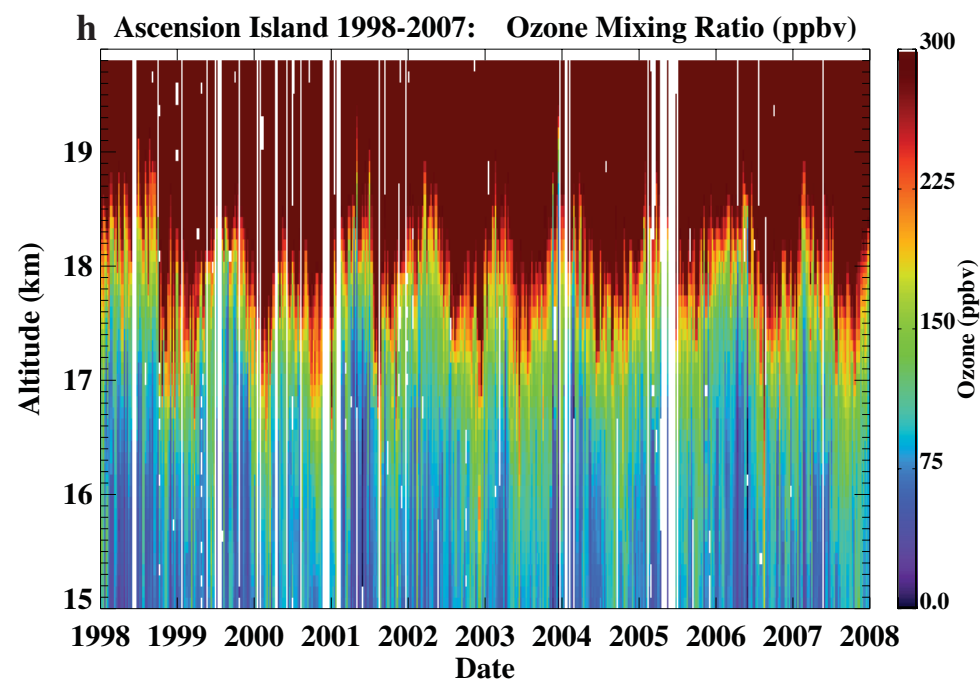
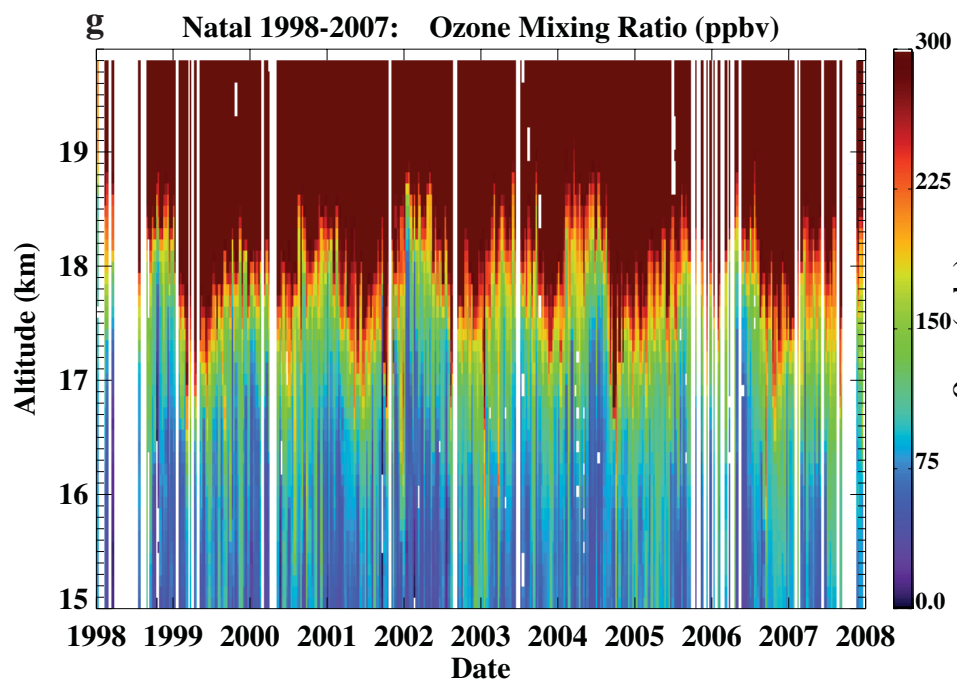
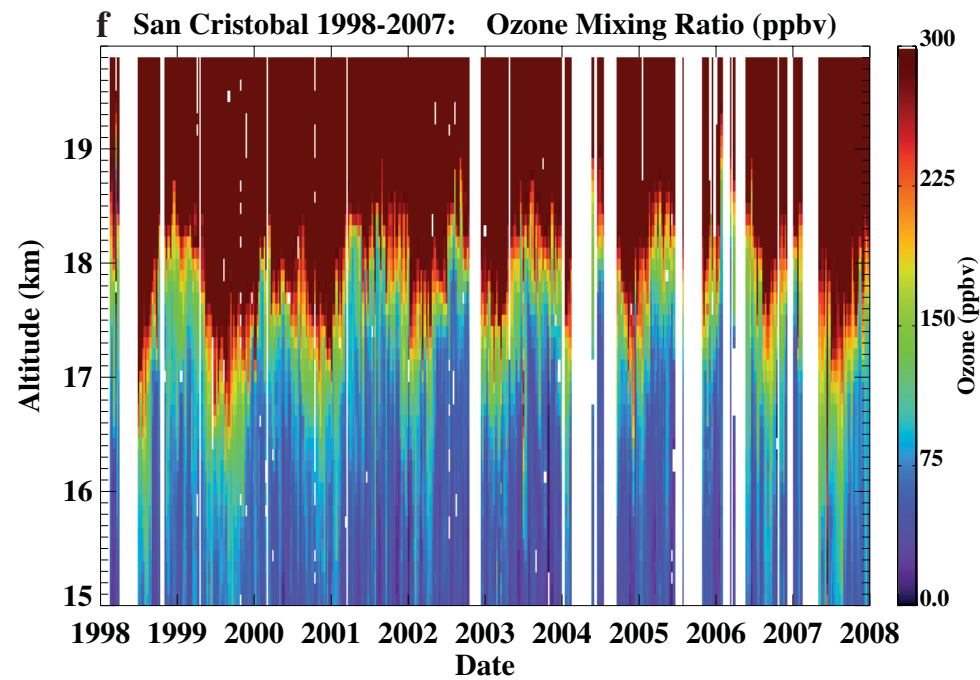
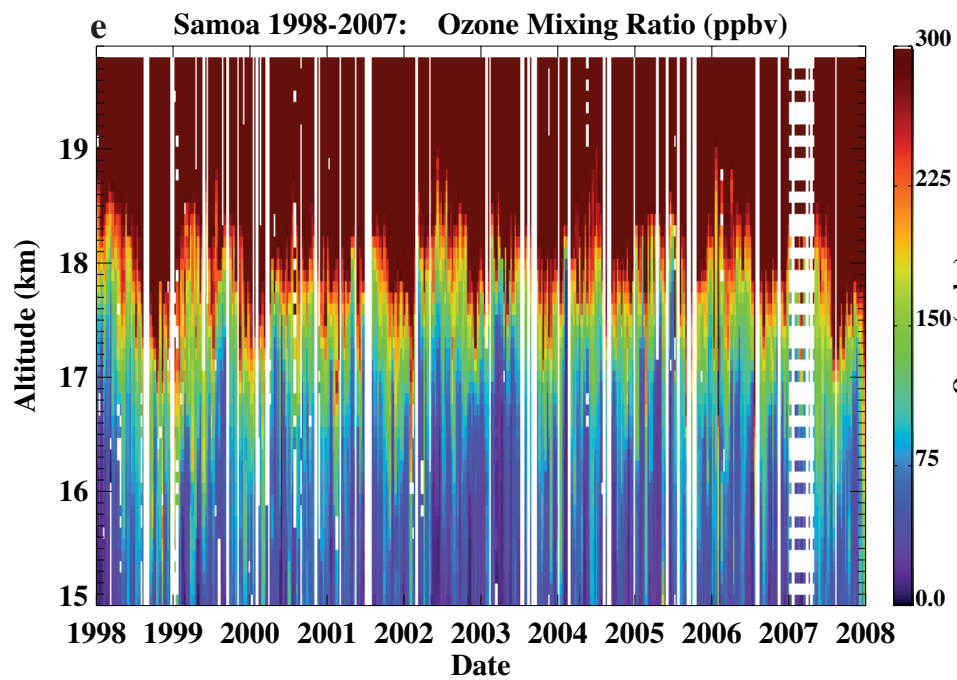


Figure S3

